HAN

Idaho National Engineering Laboratory

Managed by the U.S. Department of Energy

EG&G idaho

Work performed under DOE Contract No. DE-AC07-76ID01570

EGG-TMI-7402
November 1986

INFORMAL REPORT

CORE RELOCATION IN THE TMI-2 ACCIDENT

P. Kuan

EGG-TMI-7402

CORE RELOCATION IN THE TMI-2 ACCIDENT

P. Kuan

Published November 1986

EG&G Idaho, Inc.
Idaho Falls, Idaho 83415

Prepared for the
U.S. Department of Energy
Idaho Operations Office
Under DOE Contract No. DE-AC07-76ID01570

ABSTRACT

This report reviews the formation of the debris bed in the TMI-2 nuclear reactor core during the core damage accident on March 28, 1979, and examines plausible thermal and mechanical failure mechanisms of the crust of the consolidated region in the debris bed that allowed molten core material to relocate to the lower plenum of the reactor vessel. Thermal interaction between molten core material and lower core support structures is analyzed. The results are consistent with a sudden failure of the crust and a brief flow of molten core material that caused little, if any, damage to the lower core support structures.

CONTENTS

ABSTRACT ii

1. INTRODUCTION 1

2. CORE DAMAGE SEQUENCE 4

3. CORE RELOCATION MECHANISMS 11

3.1 Melt-Through of the Crust 11

3.1.1 Melt-Through by Decay Heat 11
3.1.2 Rapid Oxidation of Crust 15
3.1.3 The Effect of Surface Indentations 23

3.2 Mechanical Failure of the Crust 25

3.2.1 Crust Failure Stress 26
3.2.2 Thermal Stress on the Crust 31
3.2.3 Pressure Differentials Across the Crust 35
3.2.4 Collapse of the Upper Crust 40

4. THERMAL INTERACTION BETWEEN MOLTEN CORE MATERIAL AND LOWER CORE SUPPORT STRUCTURES 42

4.1 Contact Between Molten Core Material at its Melting Point and Stainless Steel 42

4.2 The Effect of Convection in the Molten Core Material 46

5. IMPLICATIONS OF THE VARIOUS FAILURE MECHANISMS 49

6. REFERENCES 53

APPENDIX A--POWER DENSITY IN THE CONSOLIDATED DEBRIS BED A-1

FIGURES

1. Known core damage conditions 2

2. Alarm sequence of self-powered neutron detectors around 225 min 7

3. Alarm sequence of core-exit thermocouples around 225 min 8

4. Source-range monitor response, primary system pressure, and cold leg temperatures around 225 min 9

5. Hypothesized core damage configuration shortly after reactor coolant pump transient at 175 min 12

6. Geometry of radiation heat loss from idealized debris bed to cooling water 14

7. Excess radiation heat flux over surface power generation due to oxidation for three values of oxide layer thickness, δ 17

8. Solutions of the critical oxidation temperature, T_c, for oxide layer thickness, δ 20

9. Cavity radiation heat transfer model 24

10. Geometry of crack in material under applied stress 27

11. Geometry of multiple cracks in material under applied stress 30

12. Solution of thermal stress in a plate with a heat flux and internal heat generation 32

13. Primary system pressure history during the TMI-2 accident 36

14. Thermal behavior of molten core material at its melting point in contact with steel below its melting point 43

CORE RELOCATION IN THE TMI-2 ACCIDENT

1. INTRODUCTION

The loss-of-coolant accident at the Three Mile Island, Unit 2 (TMI-2) nuclear reactor on March 28, 1979, resulted in severe damage to the reactor core. In the summer of 1982, a closed-circuit television survey of the core was conducted through the openings of three control rod leadscrew support tubes. The survey revealed a cavity in the upper part of the core below which the fuel was seen in the form of a rubble bed. Subsequent probing of the rubble bed by a pointed tool showed that the rubble was fairly loose and extended downward for about 1 m. Below the rubble bed, the pointed tool encountered a hard crust. After the removal of the upper head of the reactor vessel, a video camera was lowered into the lower plenum along the downcomer in February 1985. An accumulation of core debris in the lower plenum amounting to 10 to 20 metric tons was discovered. Some of this debris was in a form resembling lava rocks, up to 0.2 m in size, much larger than any of the flow holes between the lower plenum and the core. The video also showed material solidified from a molten state and still attached to the flow distributor plate. However, structures in the lower plenum, such as the flow distributor, instrument guide tubes, and the inner liner of the vessel, whenever visible, apparently suffered little, if any, damage. Recent videos, taken in July 1986 along the core bore holes for the acquisition of core samples, not only revealed the presence of fuel rod stubs below the solid debris bed in the core, but also confirmed that molten core material had flowed down near the periphery of one side of the core. The known damage state within the reactor vessel from the 1979 accident is depicted in Figure 1.

The purpose of this study is to investigate (a) the possible failure mechanisms of the non-coolable debris formed in the core region that led to the relocation of molten material to the lower plenum, and (b) the effect of molten core material flow on the lower plenum structures. The interaction of molten core material with the lower plenum structures and the lower vessel head after the molten core material settled in the lower plenum will be investigated in a separate study. Section 2 gives an overview of the

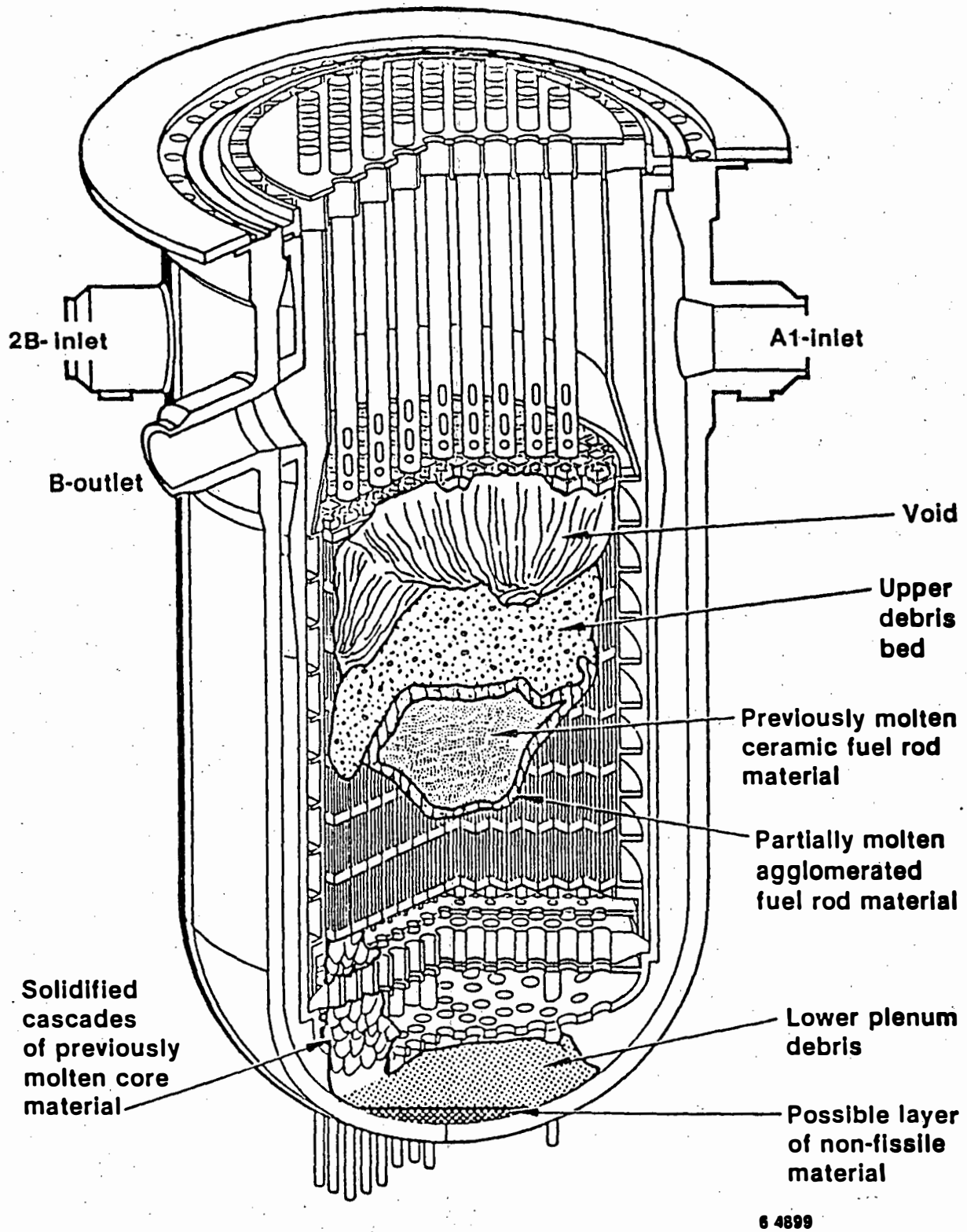

Figure 1. Known core damage conditions.

TMI-2 core damage sequence leading to the formation of a solid debris bed in the core and the final relocation of molten core material to the lower plenum. The early phases of the damage sequence up to the formation of a debris bed in the core have been modeled extensively by the severe fuel damage computer code SCDAP[1] and simulated in the severe fuel damage tests performed in the Power Burst Facility.[2,3,4,5] There is little doubt as to the general validity of the damage sequence up to core debris bed formation. The mechanism of molten core material relocation to the lower plenum, however, is poorly understood and open to various conjectures and hypotheses. Section 3 examines in detail some of the proposed mechanisms that allowed molten material to flow to the lower plenum, due to either a melt-through or a mechanical failure of the crust enclosing the molten material. Section 4 explores the effect of molten core material on the lower core support structures during its downward flow. Finally, in Section 5, the different failure mechanisms are reviewed, summarized, and related to the configuration of the debris bed and the damage state of the lower core support structures.

2. CORE DAMAGE SEQUENCE

The TMI-2 accident was initiated by the loss of main, as well as emergency, feedwater to the secondary sides of the steam generators. Due to this loss of heat sink, the primary coolant system heated up and the buildup in pressure pushed open a relief valve on the pressurizer. The reactor was shut down automatically on high pressure, but the relief valve failed in a stuck-open position. Primary coolant was lost through the stuck-open valve for more than 2 h until the pressure relief line was isolated by closing a block valve. During this time, the coolant could have been replenished by emergency core cooling water. Unfortunately, the high water-level indication in the pressurizer gave the operators an erroneous notion that the system was still full of water. Accordingly, the operators drastically curtailed the injection of emergency core cooling water, which led to the core being uncovered (water level dropping below the top of the core) at about 110 minutes into the accident.

After the core was uncovered and during the period the core coolant was being boiled off, based on the SCDAP analysis,[1] the uncovered part of the fuel rods would have heated up at a rate between 0.3 to 0.5 K/s from decay heat. Because radiation was detected in the containment a few minutes after the block valve closure at 140 min, the cladding of some of the rods must have ruptured by this time and released some fission gas. From calculations and experiments, the temperature at which the cladding would rupture is known to be between 1100 and 1200 K. After rod rupture, the two-sided rods would have heated up at an accelerated rate due to the increasing exothermic oxidation of the zircaloy cladding by steam at high temperatures.

Based on estimated heatup rates, the maximum cladding temperature would have reached 1600 K by about 160 min. At this temperature the local power output due to cladding oxidation by steam would have been several times the local decay power. Because the oxidation rate increases exponentially with the increase in temperature, the temperature of the fuel rods would have escalated rapidly, limited only by the steam or zircaloy availability. In the meantime, the stainless steel cladding of the control rods would have melted at about 1700 K and the molten control material (an alloy of silver,

indium, and cadmium that melts around 1200 K) would have been released and flowed toward the lower end of the core. Because molten silver can dissolve a considerable amount of zircaloy, it probably would have destroyed the zircaloy guide tubes of the control rods and some nearby fuel-rod cladding during its downward flow. After the zircaloy cladding melted at about 2100 K, which would have taken place only a few minutes after the cladding temperature had reached 1600 K, the molten zircaloy would also flow toward the lower end of the core. The exact temperature at which the molten zircaloy would relocate, however, is quite uncertain because of the presence of a protective layer of zirconium dioxide, which remains solid up to 2900 K. Experiments at the Power Burst Facility indicated that the relocation temperature could be as high as 2500 K, a few hundred K above the melting point of zircaloy. While the temperature was below 2700 K, the liquid cladding, based on the U-Zr-O equilibrium phase diagram, could dissolve up to 20% of the fuel it enclosed. The liquid material would fall downwards, either freely or along the fuel rods, until solidification took place in a sufficiently cool region. From the post-accident core examination, the lowest point where the molten material solidified was about 0.4 m above the bottom of the active core, roughly the estimated location of the water level during this phase of the accident. The relocated material soon would have formed a crust that provided support to subsequently relocated material. As more material melted, flowed down, and solidified, the solid region probably grew to about 1 m thick by about 170 min in the central part of the core. On top of the solid mass, there would have been the fuel-rod remnants with their oxidized cladding.

At 174 min one of the reactor coolant pumps, which were turned off earlier during the accident due to excessive vibration, was turned on and momentarily pumped a large quantity of water into the core. This could have shattered the fuel-rod remnants and the oxidized cladding in the upper part of the core to form a rubble bed. The cooling effect of the pump was transitory, and only the peripheral fuel assemblies were temporarily cooled. This was indicated by the responses of the core-exit thermocouples which ~~came back~~ failed from an alarm state at temperatures above 644 K, 700F and then again went into an alarm state when the temperature exceeded 644 K. After 200 min, emergency cooling water was injected into the reactor core.

Thermocouples in the peripheral assemblies again responded to the cooling water, but the thermocouples in the central assemblies remained in a high-temperature alarm state. It is believed that the central thermocouples formed new junctions within the solid debris bed that shielded them from the cooling water. A transient calculation of the heatup of the debris showed that, by 225 min, 12,000 kg of core material inside a crust could have remelted from decay heat.[6]

At about 225 min, several simultaneous events indicated a major change in core configuration. Many of the in-core self-powered neutron detectors (SPNDs) alarmed due to abnormally high or low currents. Careful examination of the alarm data showed that the alarms first went off in the east quadrant of the core and then propagated toward the center (as shown in Figure 2). Some of the alarms came from the same instrument stalks, each of which had seven detectors evenly spaced along the vertical axis, and a leadwire without a detector serving as a background indicator. A few of these instrument stalks had alarms from all seven levels of detectors as well as from the background leadwire. A few of the core exit thermocouples also alarmed at high temperature, following a similar sequence as the SPNDs, i.e., starting from the east quadrant of the core and propagating toward the center (as shown in Figure 3). The count rate of a neutron source-range monitor located on the outside of the reactor vessel increased sharply, and then decayed slowly. A primary system pressure pulse of about 2 MPa was recorded. The best indication of the sudden change perhaps came from the recorded temperature in the inlet piping (cold legs) of the primary coolant circulation loops. The data provide a 3-s time resolution and show that the temperatures jumped up by as much as 80 K (A-loop cold leg) in 12 s. (The time resolution of the source-range monitor output and the primary pressure is estimated to be about 1 min from the microfilms of copies of the respective strip-chart recordings.) The source-range monitor response, the primary system pressure, and the cold leg temperatures are shown in Figure 4.

loop closed

The discovery of core material in the lower plenum and an apparent flow path of molten material in the east quadrant of the core (see Figure 1), together with the events around 225 min during the accident, strongly

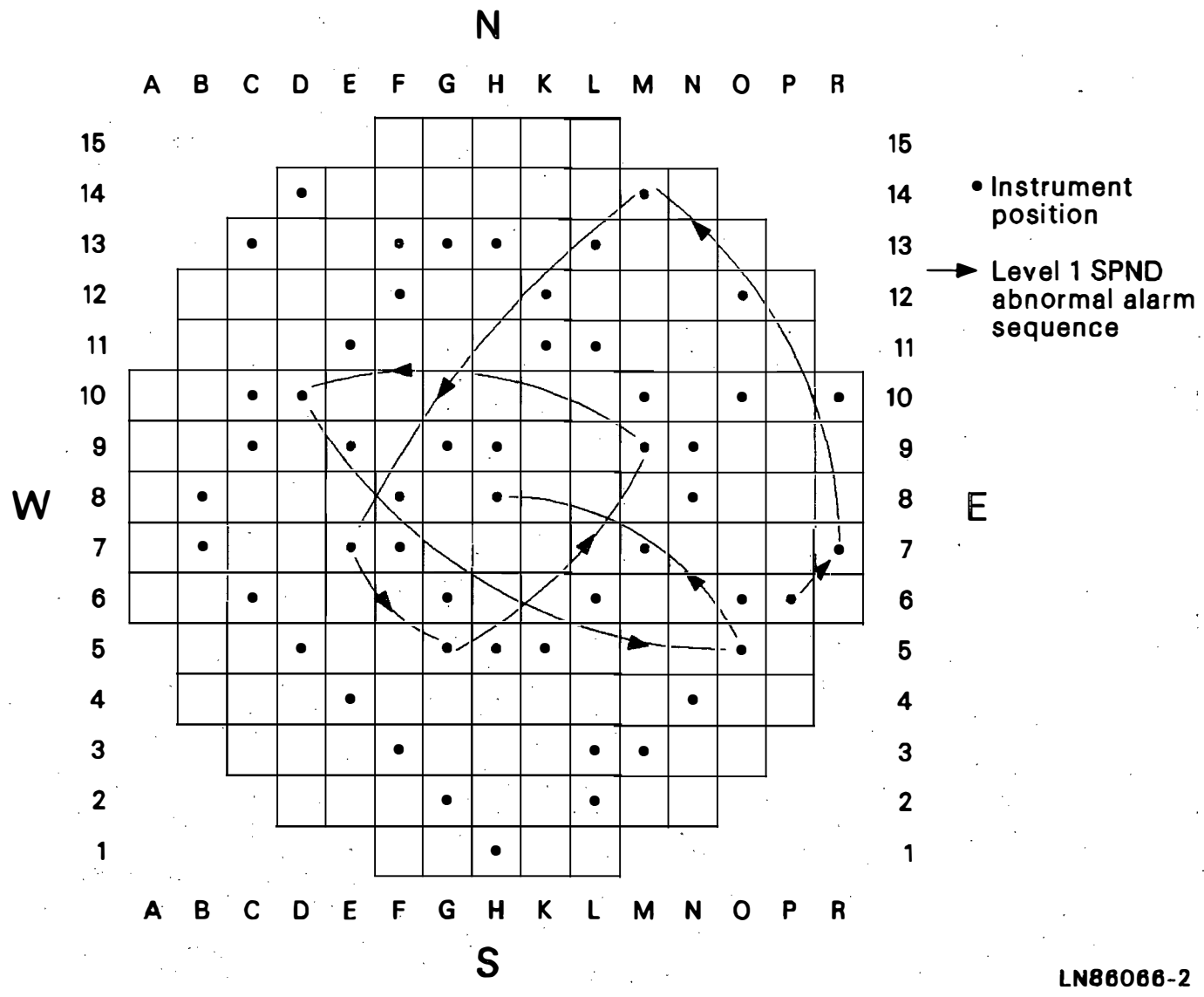

Figure 2. Alarm sequence of self-powered neutron detectors around 225 min.

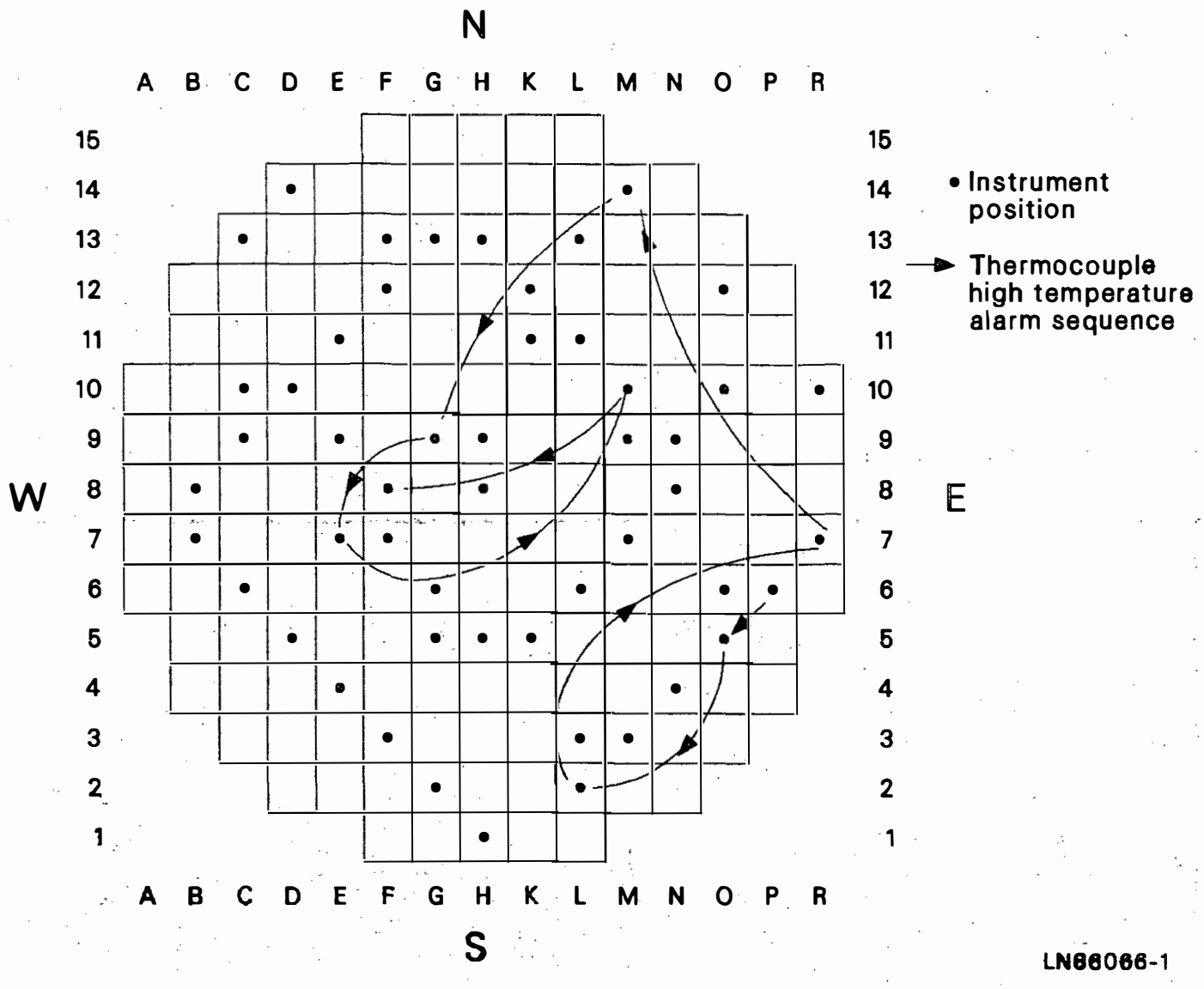

Figure 3. Alarm sequence of core-exit thermocouples around 225 min.

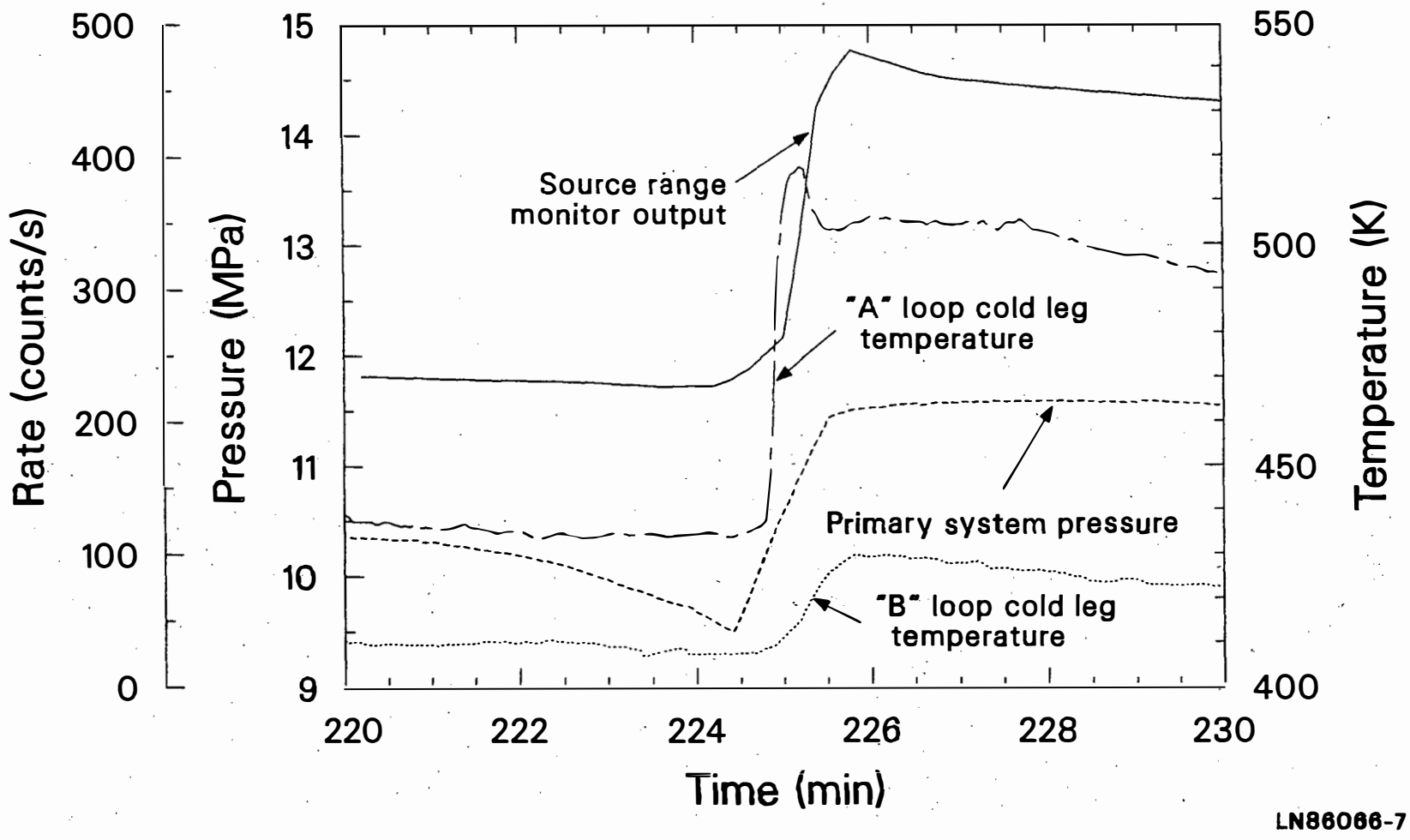

Figure 4. Source-range monitor response, primary system pressure, and cold leg temperatures around 225 min.

indicate that molten material relocated to the lower plenum at that time. The sudden increase in neutron count rate at the source-range monitor can be explained by neutron streaming from the bottom of the reactor vessel when a significant amount of fuel fell to the lower plenum.[7,8] The subsequent slow decay in the count rate can be attributed to the decay of neutron generation from a fixed fuel distribution in the reactor vessel. The simultaneous alarms of SPNDs at all levels, including the background leadwire, on the same instrument stalks, suggest a common point of damage to these instruments. If molten material flowed to the lower plenum and settled around the instrument tubes, the leadwires inside the tubes could have heated to high temperatures and developed enough thermoelectric currents to set off the alarms.[9] Post-accident measurements of the loop resistances of the core-exit thermocouples showed that new junctions were formed in the lower plenum, presumably from fusing the thermocouple leads at high temperatures.[10] The sudden increase in primary system pressure can be explained by the generation of large quantities of steam when hot core material came into contact with the cooling water. The increase in cold leg temperatures can also be explained by a sudden flow of water heated by steam from the lower plenum to the cold legs immediately after the hot core material relocated to the lower plenum.

After the hypothesized relocation event around 225 min into the accident, there was little indication of another major core configuration change. When one of the reactor coolant pumps was restarted some 16 h after the beginning of the accident, the small-sized loose debris could have been moved by the rapidly flowing water. This may have changed the surface distribution of the debris, but the main damage pattern discovered in the post-accident examination of the vessel interior is believed to have been formed immediately after the 225-min event. The evaluation of core relocation mechanisms given in the next section is aimed at finding a cause for the hypothesized relocation event at 225 min.

3. CORE RELOCATION MECHANISMS

After the reactor coolant pump transient at 174 min, the reactor core configuration can be thought of as consisting of four distinct regions as shown in Figure 5. These regions are: (1) the periphery of the core where the fuel assemblies suffered little damage and remained mostly intact in the upright position; (2) the lower end of the core, near and below the water level, where the fuel rod stubs remained standing and provided support to the resolidified material relocated from above; (3) a central consolidated region, averaging about 0.9 m in height, which was impervious to cooling water and whose interior continued to heat up from decay heat and eventually became molten; and (4) a rubble bed above the solid region, consisting mostly of shattered fuel pellets and oxidized cladding. The rubble bed could have been relatively loose and porous and, if any water was delivered to it, it eventually would be quenched. This is believed to be the case when emergency cooling water was injected into the core shortly after 200 min. With cooling water covering the reactor core, the only region that could lead to further configuration change was the consolidated, non-coolable region just below the rubble. For the molten material to relocate to the lower plenum, the crust around it must first fail. The following subsections discuss the potential failure mechanisms of the crust, under the category of a melt-through or a mechanical breakup.

3.1 Melt-Through of the Crust

3.1.1 Melt-Through by Decay Heat

If the surface temperature of the consolidated debris bed (region 3 in Figure 5) was heated above the Leidenfrost point (~900 K) at the time of emergency core coolant injection, its surface would not have been rewetted by the cooling water. At high temperatures, the heat loss from the surface would have been dominated by radiation to the cooling water through a thin film of steam. If heat carried away by the steam is neglected and only radiation loss to the water is considered, an upper bound to the equilibrium surface temperature, T_s, can be easily estimated. We assume that the debris is in the form of a right-circular cylinder, having radius, r, and height,

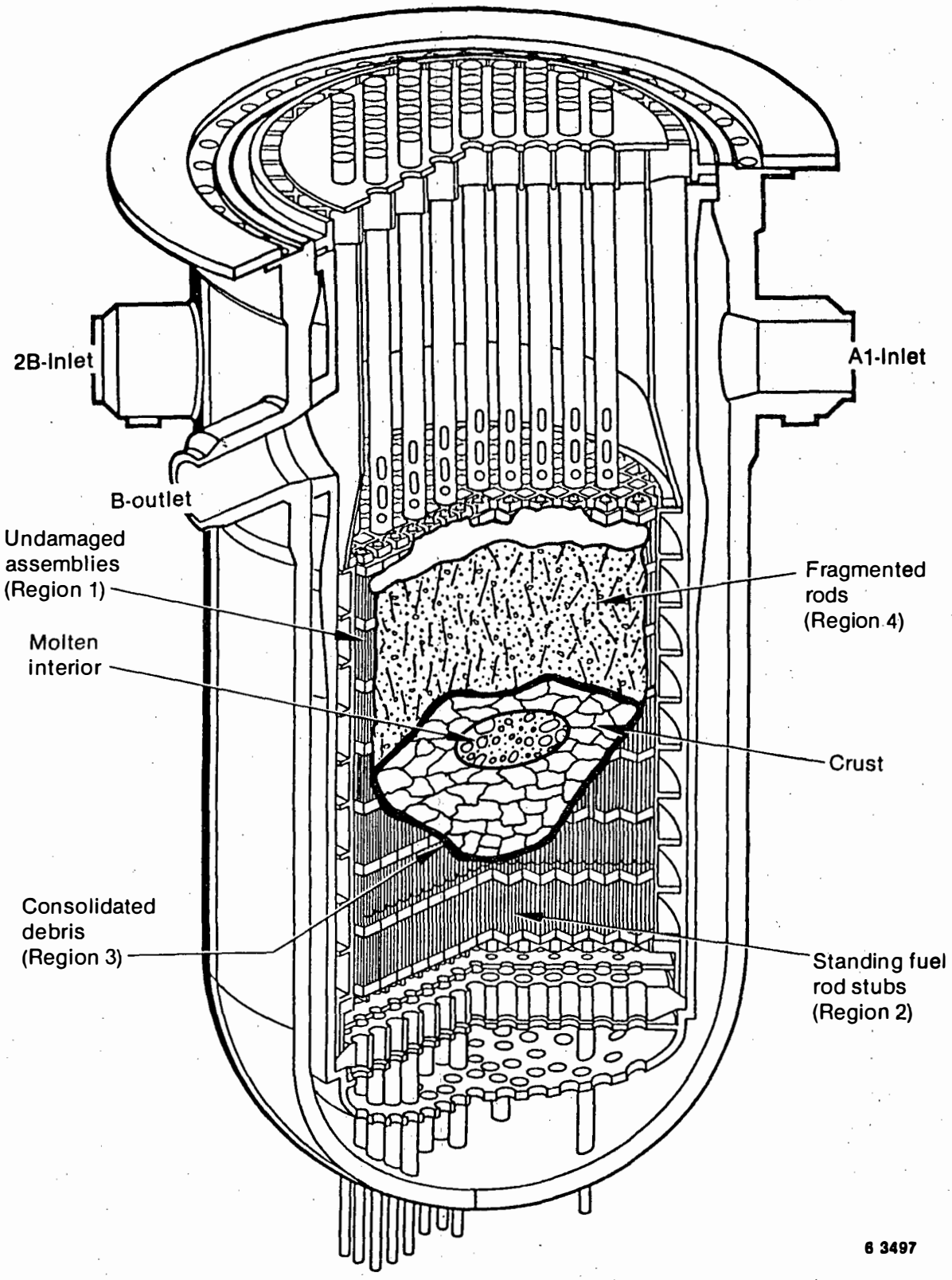

Figure 5. Hypothesized core damage configuration shortly after reactor coolant pump transient at 175 min.

h. Heat is generated in the interior from a uniform volumetric source, q''', and lost uniformly through the surfaces of the cylinder. The configuration of the problem is shown in Figure 6. Neglecting heat transfer to the steam film and back radiation from the cooling water, we have

$$q''' \cdot \pi r^2 h = \varepsilon\sigma T_s^4 (2\pi r^2 + 2\pi r h) \tag{1}$$

where ε is the emissivity, σ the Stefan-Boltzmann constant, and the other parameters as defined in the text. Solving for the surface temperature, we have

$$T_s = \left[\frac{r h q'''}{2\varepsilon\sigma(r + h)}\right]^{1/4} \tag{2}$$

Substituting the following values for the parameters estimated for the TMI-2 consolidated debris bed:

r = 1.2 m

h = 0.9 m

q''' = 1.5 MW/m^3 (see Appendix A)

ε = 0.8 (for UO_2)

σ = 5.67×10^{-14} $MW/m^2\text{-}K^4$,

we get

T_s = 1710 K .

If the surface of the debris was covered with a layer of control material, it would be melted before thermal equilibrium was reached. If the surface was made of zircaloy, there was a potential for rapid oxidation, supplying additional heat to the surface. The effect of the oxidation on

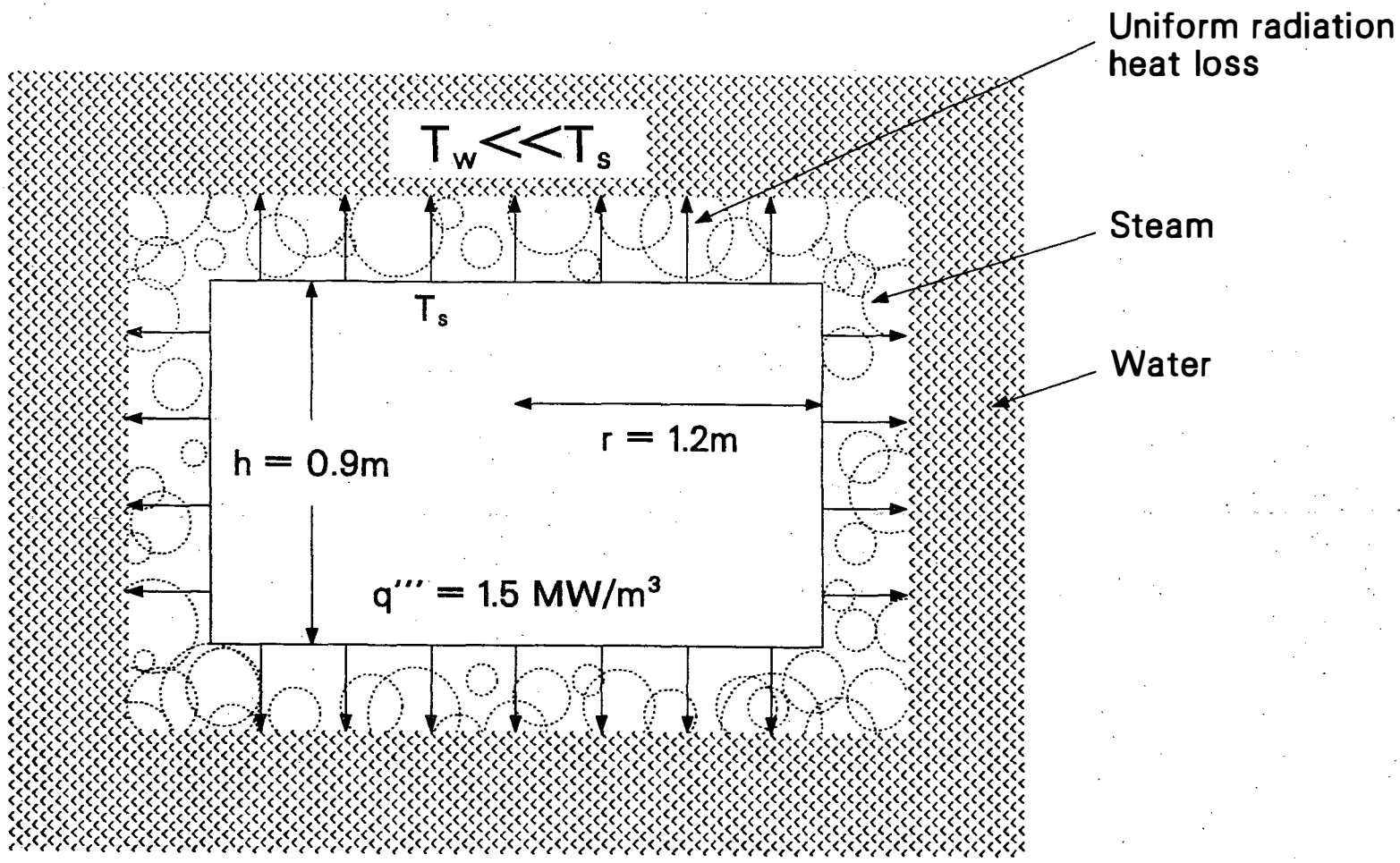

Figure 6. Geometry of radiation heat loss from idealized debris bed to cooling water.

the surface temperature is analyzed in Section 3.1.2. In the absence of oxidation, the zircaloy on the surface would be below its melting point. If the surface contained stainless steel, a melt-through was possible, because the estimated equilibrium surface temperature is in the neighborhood of its melting point. A ceramic surface, whether of ZrO_2, U-Zr-O, or UO_2, would remain solid and a melt-through was not possible, given the estimated TMI-2 debris bed decay heat generation rate and the assumption of uniform surface heat flux.

3.1.2 Rapid Oxidation of Crust

The last section showed that the surface temperature of the consolidated debris bed could be close to 1700 K. If a layer of zircaloy covered the surface, oxidation of the surface by steam could be fairly rapid. This section determines the conditions that can lead to an escalation of the crust surface temperature due to the exothermic chemical reaction, or conversely, the conditions for stable surface oxidation.

Oxidation of zircaloy by steam can be represented by the following kinetics giving the zirconium oxidized per unit surface area:

$$2W\,dW = 294.3 \exp\left\{-\frac{20,100}{T_s}\right\} dt \quad , \quad T_s < 1850 \text{ K} \tag{3a}$$

$$= 87.9 \exp\left\{-\frac{16,610}{T_s}\right\} dt \quad , \quad T_s \geq 1850 \text{ K} \tag{3b}$$

where

W = the zirconium that would be oxidized on the surface, in units of kg/m^2, if all the oxygen uptake was used to oxidize the zirconium to ZrO_2

T_s = surface temperature in K

t = time in s.

Below 1850 K, the kinetics is from Pawel et al.,[11] and at, and above, 1850 K, the kinetics is from Urbanic and Heidrick.[12] In the above equation, dW is the increment in W during the time increment dt. Using a heat generation of 6.45 MJ when 1 kg of zirconium is oxidized and a zirconium density of 6500 kg/m^3, the surface power generation, P_s, can be derived from the above kinetics as

$$P_s = \frac{\alpha}{\delta} \exp\left(-\beta/T_s\right) \tag{4}$$

$$= \frac{1.46 \times 10^5}{\delta} \exp\left\{-\frac{20,100}{T_s}\right\} (\mathrm{MW/m^2}) \quad , \quad T_s < 1850 \text{ K} \tag{4a}$$

$$= \frac{4.36 \times 10^4}{\delta} \exp\left\{-\frac{16,610}{T_s}\right\} (\mathrm{MW/m^2}) \quad , \quad T_s \geq 1850 \text{ K} \tag{4b}$$

where

δ = the thickness in micrometers of the original zirconium layer that has been oxidized if all the oxygen uptake is absorbed in this layer.

If we define $f(T_s)$ as

$$f(T_s) = \varepsilon\sigma T_s^{\,4} - P_s \quad , \tag{5}$$

where the first term on the right-hand side is the heat flux due to radiation loss and P_s, the surface power generation due to oxidation, then $f(T_s)$ is the excess heat flux from the surface. (Convective heat flux has been ignored.) If T_s is to be constant in time, $f(T_s)$ has to be balanced by the heat flux from the interior. The function f is shown in Figure 7 for three values of the oxidized zircaloy layer thickness, δ.

The function, f, apart from the discontinuity at 1850 K, has in general a maximum value and also a minimum value at a higher temperature (not shown

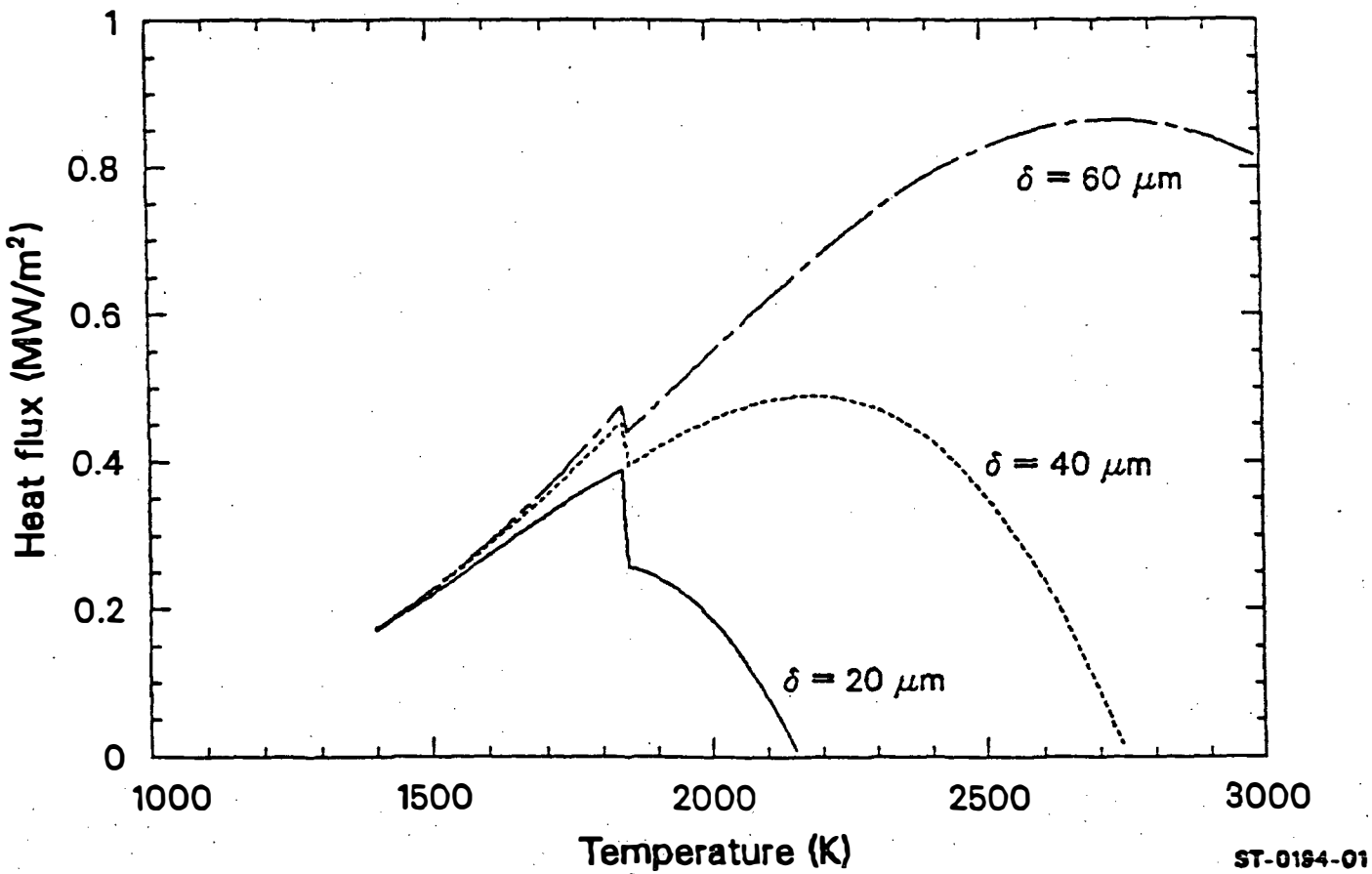

Figure 7. Excess radiation heat flux over surface power generation due to oxidation for three values of oxide layer thickness, δ.

in Figure 7). If the heat flux from the interior is higher than the maximum, equilibrium is not possible at low temperatures and the temperature of the surface escalates. If the heat flux from the interior intercepts the f-curve to the left of the maximum, the oxidation is stable, because a slight increase in temperature means an increase in net cooling, causing the temperature to drop back. If the intercept is to the right of the maximum, oxidation is unstable, and the temperature escalates until it moves over to the right of the minimum on the f-curve. The condition of stable oxidation is, therefore,

$f'(T_s) > 0$, or

$$4\varepsilon\sigma T_s^{\,3} - \frac{\alpha\beta}{\delta T_s^{\,2}}\, e^{-\beta/T_s} > 0 \quad , \tag{6}$$

where α and β are the constants shown in Equation (4).

Setting $f'(T_s) = 0$, we obtain the upper bound on the surface temperature, T_c (later referred to as the critical temperature), for stable oxidation:

$$T_c^{\,5} = \frac{\alpha\beta}{4\varepsilon\sigma\delta}\, e^{-\beta/T_c} \quad , \tag{7}$$

and this has to be supplemented by the condition that $f''(T_c) < 0$.

The temperature in the Cathcart-Pawel oxidation regime extends to 1850 K. If this is set to T_c, we obtain from Equation (7), after substituting the values

α = 1.46×10^5 MW-μm/m^2

β = 20,100 K

ε = 0.8

$$\sigma = 5.67 \times 10^{-14}\ MW/m^2\text{-}K^4,$$

$$\delta = \delta_c = 14.3\ \mu m \quad . \tag{8}$$

For $\delta < \delta_c$, the Inequality (6) cannot be satisfied and the temperature will escalate to the Urbanic regime ($T_s > 1850$ K). For $\delta > \delta_c$, the oxidation is stable for any temperature below 1850 K.

In the Urbanic regime, the critical temperature, T_c, as a function of the thickness of the oxidized zircaloy, is obtained by numerically solving Equation (7), and is given below in tabular form:

$\delta(\mu m)$	25	30	35	40	50	60
$T_c(K)$	1885	1984	2082	2184	2413	2731

Equation (7), as given above for the temperature at which the f-curve has a stationary value, generally has two solutions in the Urbanic regime for a given value of δ. This is graphically illustrated in Figure 8. The lower temperature gives the location of the maximum on the f-curve and the upper temperature the minimum. As δ is increased, the two solutions eventually coincide at $\delta = \delta_c'$, and for $\delta > \delta_c'$, the function f is a monotonically increasing function of T_s. Thus, δ_c' gives the thickness of the oxidized zircaloy above which oxidation of the zircaloy is stable at any temperature. (As shown below, this also applies to the Cathcart-Pawel regime.)

The point $\delta = \delta_c'$ is determined by the solution of the following equation:

$$\frac{d\delta}{dT_c} = 0 \quad . \tag{9}$$

Differentiating Equation (7), we have

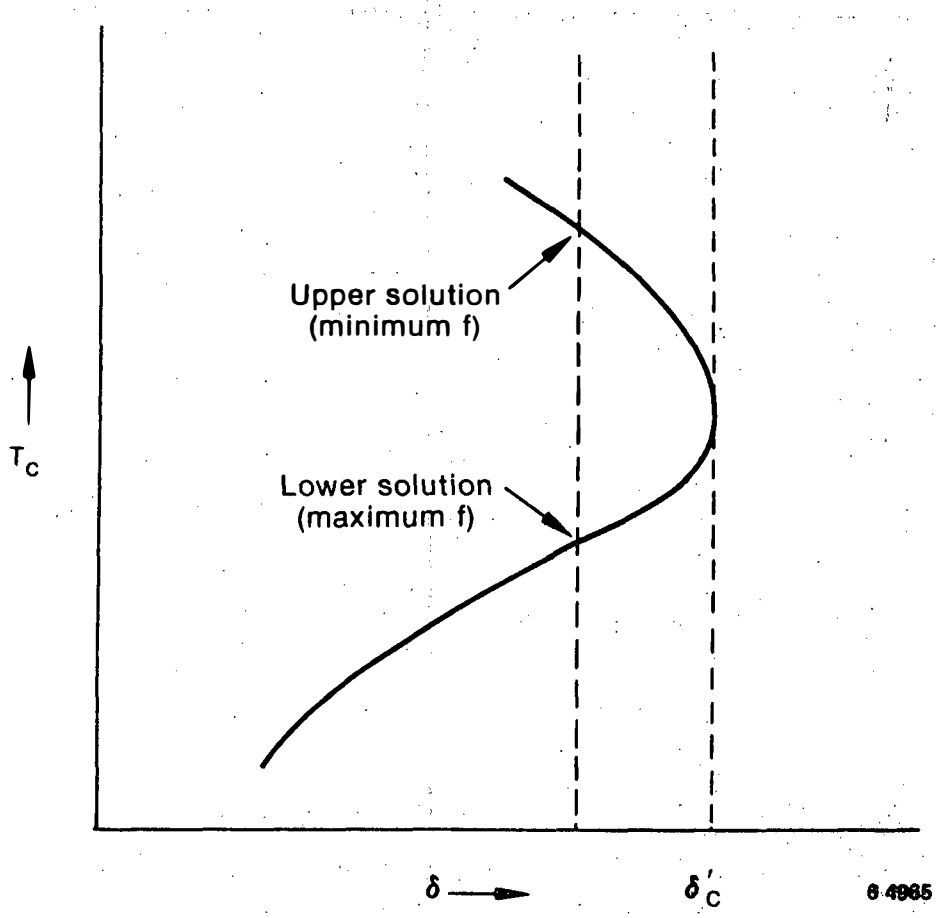

Figure 8. Solutions of the critical oxidation temperature, T_c, for oxide layer thickness, δ.

$$5T_c^{\,4}\, dT_c = \frac{\alpha\beta}{4\varepsilon\sigma}\, e^{-\beta/T_c} \left[-\frac{1}{\delta^2}\, d\delta + \frac{\beta}{T_c^{\,2}\delta}\, dT_c \right]$$

$$= -\, T_c^{\,5} \left[\frac{d\delta}{\delta} - \frac{\beta}{T_c^{\,2}}\, dT_c \right] \quad , \tag{10}$$

from which we get

$$T_c = \beta/5 \quad , \tag{11}$$

by setting $d\delta/dT_c = 0$. Substituting this value of T_c into Equation (7) again, we get

$$\delta_c' = \frac{5^5\alpha}{4\varepsilon\sigma\beta^4}\, e^{-5} \quad . \tag{12}$$

Substituting the numerical values

α = 4.36×10^4 MW-μm/m^2

β = 16,610 K

ε = 0.8

σ = 5.67×10^{-14} MW/m^2-K^4,

we obtain

$$\delta_c' = 66.5\ \mu m \quad . \tag{13}$$

Because this is larger than the critical thickness, δ_c, obtained for the Cathcart-Pawel regime, as given by Equation (8), the oxidation is stable at all temperatures if the oxidized zircaloy thickness is more than δ_c', or 66.5 μm.

For a cylindrical debris bed, 0.9 m high and 1.2 m in radius, and having a volumetric power density of 1.5 MW/m^3, the average equilibrium surface heat flux due to the internal heat generation, as estimated in Section 3.11, is about 0.4 MW/m^2. If the initial oxidized zircaloy thickness is more than about 15 μm, the oxidation is stable and the surface temperature will remain below 1850 K. In particular, the equilibrium surface temperature will be about 1750 K when the oxidized layer reaches 40 μm.

If the initial oxide layer is less than 15 μm, the temperature may escalate above 1850 K. The temperature escalation, however, will be of short duration, for the oxide layer will build up rapidly and the temperature will subsequently drop. The time, τ, to oxidize a layer of thickness, δ, from $\delta = 0$ is given by the integral of Equation (3) after converting W to δ, i.e.,

$$\tau = \frac{\rho^2 \delta^2}{\alpha} e^{\beta/T_s} , \tag{14}$$

where α and β are as defined in Equation (4) and

ρ = the density of zircaloy (6500 kg/m^3).

For $T_s > 1850$ K, the time τ is numerically given by

$$\tau = 4.81 \times 10^{-7} \delta^2 e^{16,610/T_s} , \tag{15}$$

where δ is in μm, T_s in K, and τ in s. At 1950 K, to reach an oxidized layer of 67 μm, the time required is only 11 s.

From the above results, we conclude that the idealized TMI-2 debris bed, with a surface layer of zircaloy, may be rapidly oxidized at the surface and, except for the unusual case of suddenly exposed fresh zircaloy at high temperature, the oxidation will be stable and will not lead to a temperature escalation if the surface is allowed to radiate to a pool of

cooling water. Even in the case of sudden exposure of fresh zircaloy at the surface, the temperature escalation will be of extremely short duration and is not likely to lead to a melt-through of the crust.

3.1.3 The Effect of Surface Indentations (Based on work by Fauske and Associates)

In Section 3.1.1, the maximum surface temperature of the debris bed was calculated to be about 1710 K if the surface was flat and heat loss was by radiation to a water surface. If the surface has an indentation in it, part of the radiation from the indentation will not fall directly on the water surface, and radient heat exchange among the surface elements has to be considered.

The surface indentations could be simply surface irregularities or cavities left behind by a low-melting-point material, such as pieces of steel or Inconel (melting point ~1700 K), or remnants of control rods made of Ag-In-Cd (melting point ~1200 K). If an indentation can be approximated by a cylindrical cavity with a constant heat flux over the cylindrical surface and an insulated cap, the temperature distribution along the cavity can be obtained from the solution given by Perlmutter and Siegel[13] for a tube open at both ends to an environment at zero temperature. The temperature at the deep end of the cavity is equivalent to the temperature at the mid-section of the tube in the Perlmutter and Siegel solution. Because the surface of the debris bed is believed to be rough, we shall use the solution for diffusely reflecting gray surfaces rather than for specularly (mirror-like) reflecting gray surfaces, even though the latter is the main topic of the referenced article.

If the cylindrical cavity is of length, L, and diameter, D, and the heat flux through the cylindrical wall is a constant, q'', as shown in Figure 9, the temperature distribution, T_s, along the wall is given by

$$T_s^4 = \frac{q''}{\sigma}\left[\frac{1}{\varepsilon} + p^4 - 1\right] , \qquad (16)$$

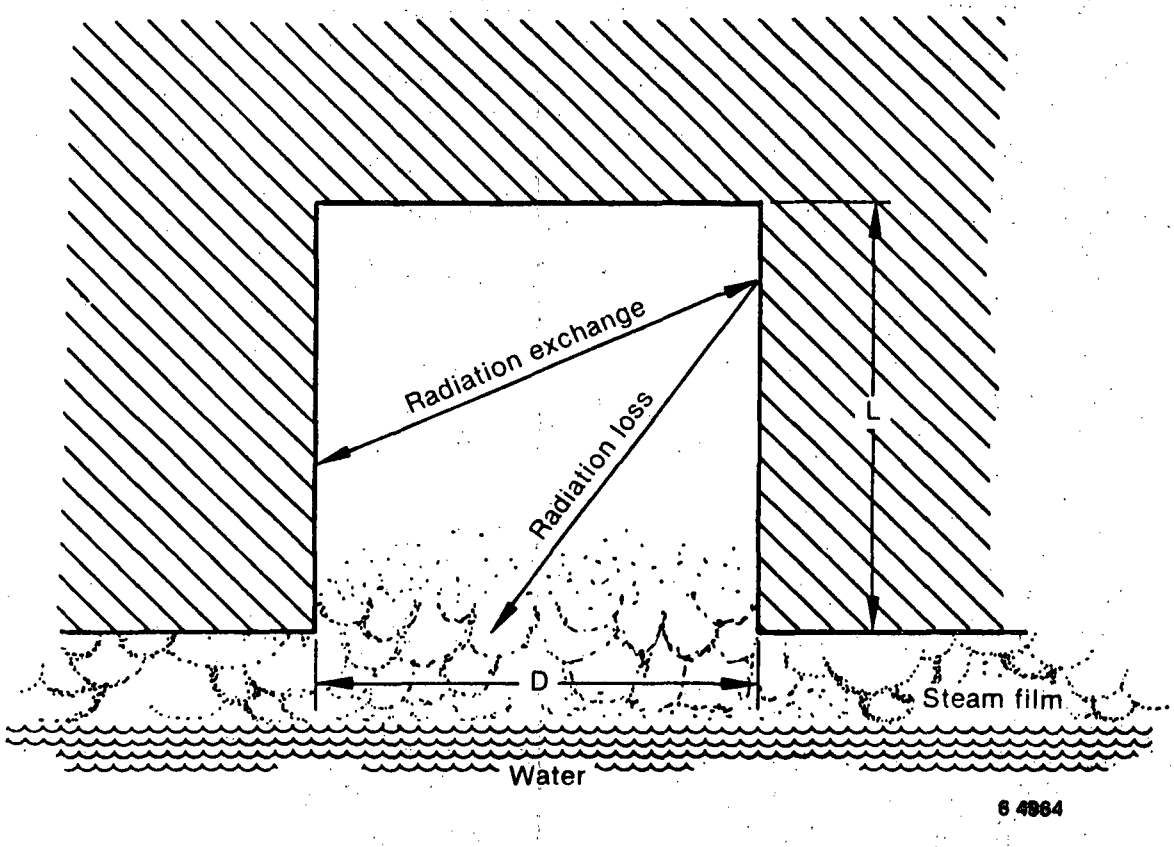

Figure 9. Cavity radiation heat transfer model.

where σ is the Stefan-Boltzmann constant, ε the emissivity, and p is a function of L/D and x/L, x being the distance measured from the open end of the cavity. For each value of L/D, p is an increasing function of x/L, so the maximum temperature is attained at the deep end of the cavity where x is largest. From the Perlmutter and Siegel[13] solution, the following maximum values of p for three values of L/D are obtained:

$$p_{max}\ (2.5) = 2.07$$

$$p_{max}\ (5.0) = 2.73$$

$$p_{max}\ (10.0) = 3.69.$$

When the above values of p_{max} are extrapolated to smaller values of L/D, bearing in mind that p is unity when L is zero, i.e., when there is no cavity, $p_{max}\ (2.0) \simeq 1.90$. With this value of p_{max}, the maximum cavity temperature for $q'' = 0.4\ MW/m^2$ and $\varepsilon = 0.8$ is calculated from Equation (16) to be 3110 K, high enough to melt UO_2. For an L/D ratio of 5, the surface heat flux required to melt UO_2 is only about 0.1 MW/m^2. Therefore, the likelihood of a crust melt-through is greatly increased in the presence of cavities on the surface of the crust.

3.2 Mechanical Failure of the Crust

In the previous section on the thermal behavior of the TMI-2 consolidated debris bed formed in the reactor core, it was found that, except for surface indentations, the equilibrium surface temperature of the crust would be less than 1700 K when the consolidated debris bed was immersed in water. Below this temperature, UO_2, or the ceramic material U-Zr-O, is well below its melting point. If the crust was composed of this material, the mechanism for its mechanical breakup probably would be through brittle fracture at sufficiently high stress levels. In the next subsection, the failure stress of the crust is estimated from the theory of brittle fracture . Two ways by which stress could develop in the crust are examined: (a) thermal stress due to a temperature gradient across the crust; and (b) stress due to a pressure differential across the crust.

These are presented in Sections 3.2.2 and 3.2.3, respectively. In section 3.2.4, the stress on the upper crust due to the weight of the rubble is examined to determine the conditions of its collapse after some molten material drained out of the debris bed.

3.2.1 Crust Failure Stress

The fracture strength of materials is often several orders of magnitude less than what might be expected from molecular forces. In the Griffith theory of brittle fracture,[14] this is attributed to the presence of microscopic cracks in the material that produce high local stress concentrations. As the cracks open up under an applied stress, a certain amount of the strain energy in the material is released and appear as energy on the newly created surface. At the point when the strain energy release is enough to balance the surface energy creation, the cracks open up spontaneously, leading to a rapid fracture of the material.

First, consider an infinite plate of uniform thickness with a crack of length 2a embedded in it and parallel to the plane of the plate. The crack is also considered infinite in extent perpendicular to its length. A uniform stress, σ, is applied to the plate in the direction perpendicular to the plane of the plate, as shown in Figure 10. Based on elastic stress analysis, the strain energy per unit width in the plate, as compared to a plate without a crack, is reduced by an amount

$$B = \pi a^2 \cdot \frac{\sigma^2}{E} \cdot (1 - \nu^2) \quad , \tag{17}$$

where E is the Young's modulus of the material and ν the Poisson's ratio.[15,16] If the crack is extended from 2a to 2(a + δa), the further reduction in strain energy per unit width is

$$\delta B = 2\pi a \cdot \frac{\sigma^2}{E} \cdot (1 - \nu^2)\, \delta a \quad . \tag{18}$$

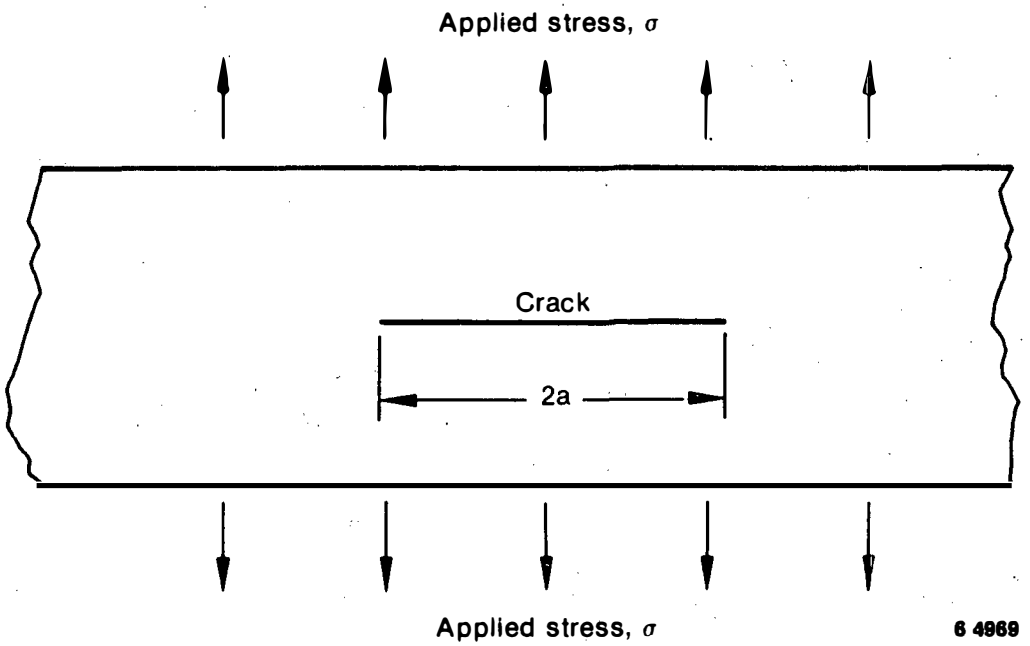

Figure 10. Geometry of crack in material under applied stress.

When this is balanced by the increase in surface energy per unit width along the crack, $2\gamma \cdot 2\delta a$, where γ is the energy per unit surface area, the crack will open up spontaneously. The factor 2 in front of γ accounts for the upper and lower surfaces of the crack and $2\delta a$ is the increase in length of the crack. If we denote σ_f the stress at which the crack opens up spontaneously, we have

$$2\pi a \cdot \frac{1 - \upsilon^2}{E} \cdot \sigma_f^2 = 4\gamma \quad , \tag{19a}$$

or

$$\sigma_f = \sqrt{\frac{2\gamma E}{\pi a \ (1 - \upsilon^2)}} \quad . \tag{19b}$$

If the plate is thin in the direction perpendicular to the length of the crack and also to the applied stress, the plate will be in plane stress and Equation (19b) is accordingly modified as

$$\sigma_f = \sqrt{\frac{2\gamma E}{\pi a}} \quad . \tag{20}$$

The derivative of B with respect to crack length extension, $\delta(2a)$, at the failure point is generally referred to as the critical energy release rate, G_c . Note that G_c has the unit of energy per unit surface area and is given by

$$G_c = 2\gamma \quad . \tag{21}$$

Because γ, or G_c, υ, and E are material properties, we have

$$\sigma_f \sqrt{\pi a} = K_c = \text{constant} \quad , \tag{22}$$

where K_c is referred to as the critical stress intensity factor.

To estimate the critical energy release rate, G_c, we use the following approximate values based on curves given in MATPRO,[19] at temperatures around 1700 K,

$$\sigma_f = 130 \text{ MPa}$$

$$E = 1.6 \times 10^5 \text{ MPa}$$

$$\nu = 0.32.$$

From Equations (19) and (21), G_c is given numerically as

$$G_c = 0.30\ a \quad (J/m^2) \quad , \tag{23}$$

where a is in micrometers.

If a is on the order of a few grain size, say 50 μm (crack length ~0.1 mm), then G is about 15 J/m^2. This also yields a critical stress intensity factor of about 1.6 MPa $\sqrt{m}$, which is within the range of the critical stress intensity factors for UO_2 given in handbooks (1.4 - 2.0 MPa $\sqrt{m}$). In the subsequent analysis, the value of 15 J/m^2 will be used for G_c.

If the crust of the TMI-2 debris bed in the reactor core was formed from relocated material solidified between fuel rods, the contact between the relocated material and the fuel-rod cladding might not be completely consolidated. The fuel rods in this case may be considered as cracks in the crust in the analysis of fracture failure. For cracks of length 2a, spaced 2h apart in the direction perpendicular to the applied stress (Figure 11), Hasselman[18] gives the following formula for the failure stress:

$$\sigma_f = \left[\frac{E G_c}{2h\ (1 - \nu^2)} \cot\left(\frac{\pi a}{2h}\right) \right]^{1/2} . \tag{24}$$

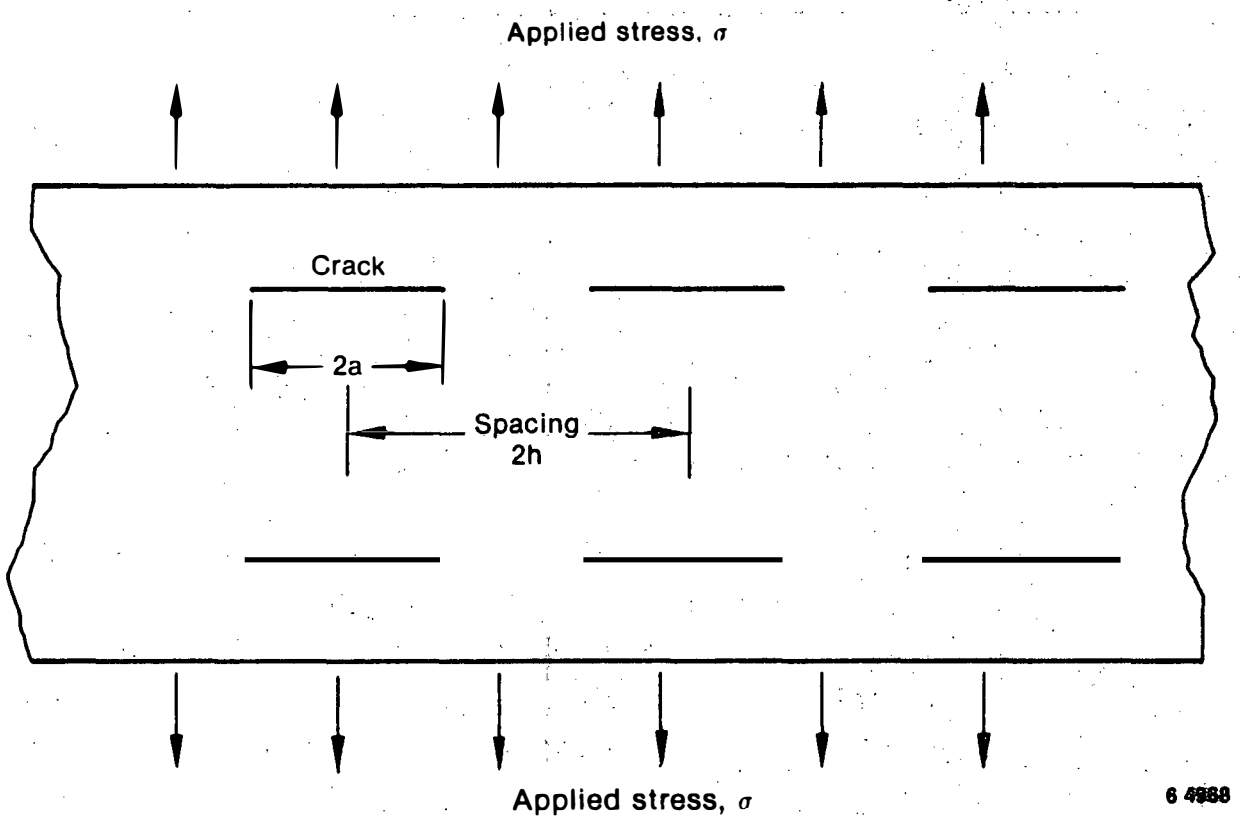

Figure 11. Geometry of multiple cracks in material under applied stress.

As the spacing goes to infinity ($h \rightarrow \infty$), the failure stress given above reduces to the failure stress for a single crack of length 2a, given by Equation (19).

The diameter, 2a, of a fuel rod is 10.9 mm and the fuel rod pitch, 2h, is 14.4 mm. Substituting these values in Equation (24), we obtain

$$\sigma_f = 8.6 \text{ MPa} \quad . \tag{25}$$

For a single crack of length 10.9 mm, the failure stress based on Equation (19b) is

$$\sigma_f = 12.5 \text{ MPa} \quad . \tag{26}$$

Both of the above failure stresses are an order of magnitude lower than the failure stress of a homogeneous sample of UO_2.

3.2.2 <u>Thermal Stress on the Crust</u> (Based on work by Fauske and Associates)

To estimate the thermal stress on the crust of the TMI-2 consolidated debris bed, we assume that the crust is in the form of a large plate of uniform thickness, 2c, and without edge constraints. Heat flux from the interior of the debris bed going into the crust is, F, and volumetric heat generation rate in the crust is, q'''. If the origin of the axis perpendicular to the plane of the plate (y-axis) is chosen at the center of the plate (see Figure 12), the stress, σ, parallel to the plane of the plate, as given by elastic analysis, is

(Reference 19)

$$\sigma = -\frac{\alpha E}{1-\nu}\left[T - \frac{1}{2c}\int_{-c}^{c} T dy - \frac{3y}{2c^3}\int_{-c}^{c} Ty dy\right] \quad , \tag{27}$$

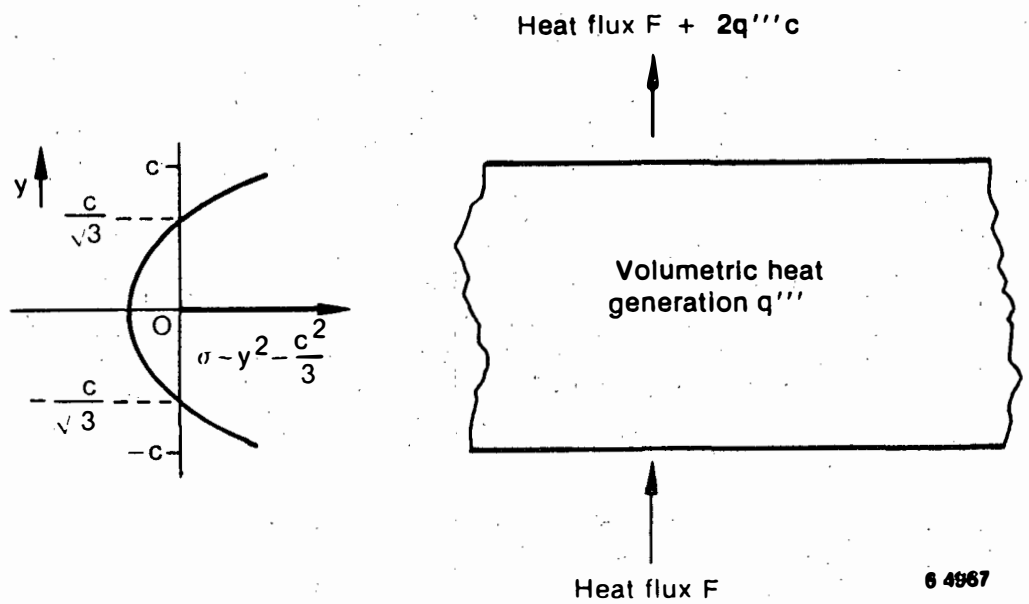

Figure 12. Solution of thermal stress in a plate with a heat flux and internal heat generation.

where

α = coefficient of thermal expansion

E = Young's modulus

ν = Poisson's ratio

T = temperature distribution.

The parameters α, E, and ν are considered constant throughout the plate.

The temperature distribution in the plate, under steady-state conditions, is given by

$$T = T_0 - \frac{q'''}{2k} y^2 - \frac{F + q'''c}{k} y \quad , \tag{28}$$

where T_0 is the temperature at the center of the plate, k the thermal conductivity, q''' the volumetric heat generation rate in the crust, and F the heat flux from the interior of the consolidated debris bed. Both k and q''' are considered constants.

If T is a constant, the first term on the right-hand side of Equation (27) cancels the second term, and the third term integrates to zero. If T is linear in y, the first term cancels the third term, and the second term integrates to zero. In either case, the stress on the plate is zero. Therefore, we need only to substitute the quadratic term in Equation (28) into Equation (27) to obtain the stress. The result is

$$\sigma = \frac{\alpha E q'''}{2k\,(1 - \nu)} \left(y^2 - \frac{c^2}{3} \right) . \tag{29}$$

The maximum stress occurs at the surfaces of the crust and is given by

$$\sigma_{max} = \frac{\alpha E q''' c^2}{3k\ (1 - \nu)} \quad . \tag{30}$$

Substituting the values representative of UO_2 (from MATPRO[17])

α = 1.4×10^{-5}/K

E = 1.6×10^5 MPa

k = 2.5 W/m-K

ν = 0.32,

we obtain

$$\sigma_{max} = 44\ q'''\ c^2\ \text{(MPa)} \quad , \tag{31}$$

where q''' is in MW/m^3 and c in centimeters.

For q''' equal to 1.5 MW/m^3, Equation (31) gives a surface stress that exceeds the failure stress of a homogeneous piece of UO_2 when the crust is more than about 3 cm thick. If the crust has embedded fuel rods, which can be considered as imperfections in the crust, as done in the last section, a thickness of more than 1 cm will create a surface thermal stress exceeding the calculated failure stress of about 10 MPa. If the heat flux through the crust is 0.4 MW/m^2, the temperature drop across the crust 1600 K, and the thermal conductivity taken as 2.5 W/m-K, the equilibrium crust thickness is 1 cm. Therefore, a crust formed from solidified material between fuel rods tends to crack at its surface, while a crust formed from solidification from a molten pool of UO_2, which is more homogeneous, may hold up against such thermal stress.

Although the outer surface of the crust may crack due to thermal stress, its interior surface may simply wrinkle due to plastic flow, because its temperature is near the melting point. The thermal stress, however,

turns compressive in the interior of the crust [σ negative for $|y|<c/\sqrt{3}$ in Equation (29)], so this will not lead to a complete failure of the crust.

3.2.3 Pressure Differentials Across the Crust

Pressure differentials across the crust can develop if the crust completely seals off its interior from the reactor coolant system. We assume that this is so in the following analysis.

There are two ways that the pressure differential can change with time. The first is by changing the pressure of the reactor coolant system. Between 200 and 224 min after the beginning of the accident, the primary system pressure dropped by about 3.4 MPa (Figure 13). If the crust is considered as a thin shell of thickness, d, and radius, R, the tangential stress, σ, on the crust is given by

$$\sigma = \frac{R}{2d} \Delta p \quad , \tag{32}$$

where Δp is the pressure differential across the crust. If the interior pressure remained constant while the reactor coolant system pressure dropped by 3.4 MPa, from Equation (32), the additional stress on the crust is

$$\delta\sigma = 1.7 \text{ R/d (MPa)} \quad . \tag{33}$$

Because R is on the order of 1 m, and d at most a few centimeters when the debris bed reaches steady-state temperatures, the increase in tangential stress is on the order of tens of MPa. If the initial pressure differential (interior pressure less external pressure) was non-negative before the external pressure drop, the additional stress from the external pressure drop would fail a crust formed from solidified material between fuel rods, but not necessarily a more homogeneous crust formed from the solidification of UO_2 in a molten pool.

Another way the differential pressure could change is through melting of the crust or solidification of the interior molten pool. A phase change

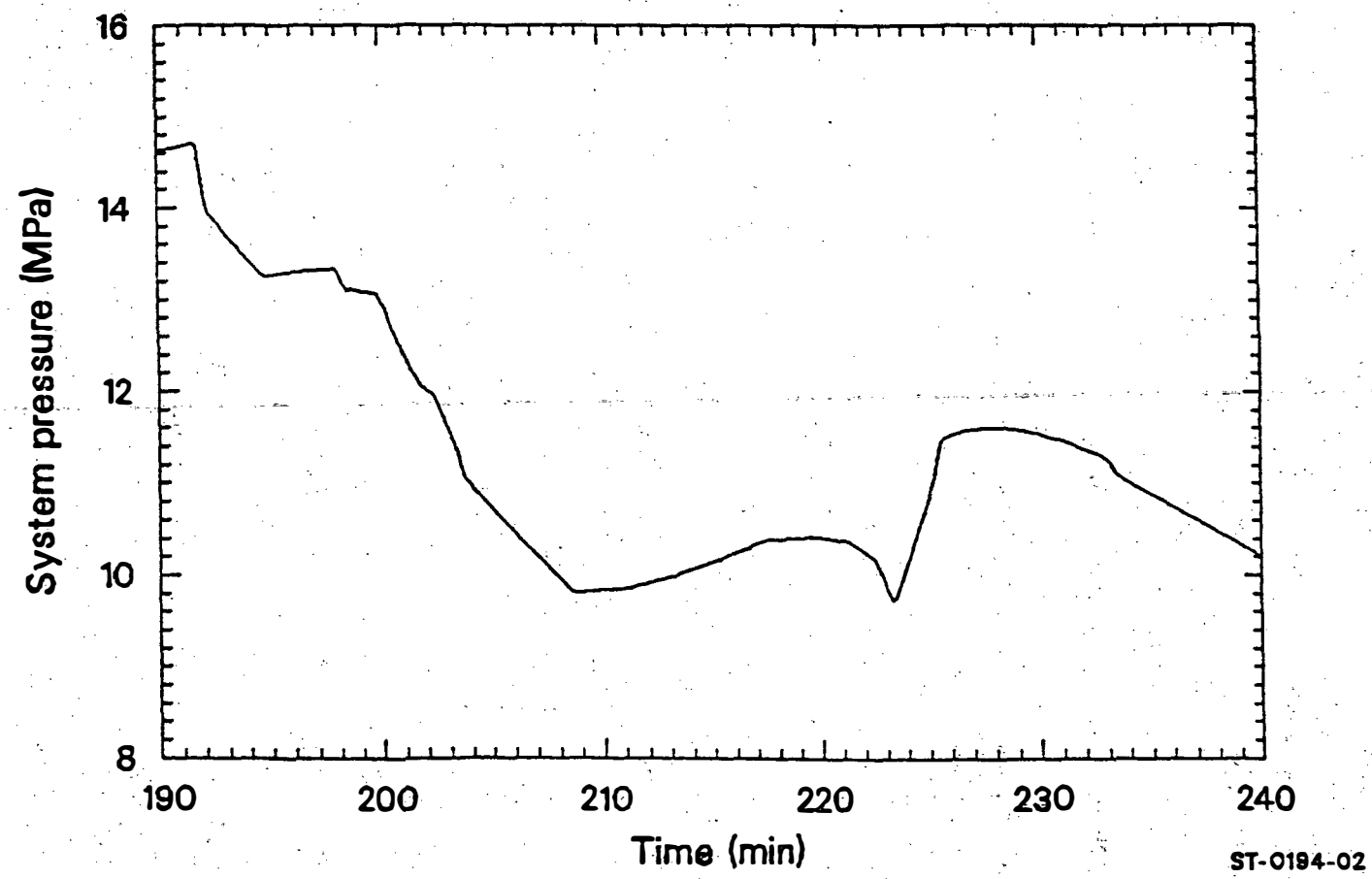

Figure 13. Primary system pressure history during the TMI-2 accident.

from solid to liquid UO_2 involves an increase in volume by about 15% under constant pressure. If the volume is constrained to change by less than 15%, the hydrostatic pressure in the liquid must change. Let E_ℓ denote the bulk modulus of liquid UO_2 (or U-Zr-O), V the volume of molten UO_2 inside the crust, and δV the volume change if an additional hydrostatic pressure δp is applied to it. Then,

$$\delta p = E_\ell \delta V/V \quad . \tag{34}$$

The increase in internal pressure causes the radius of the crust to expand by an amount

$$\delta R = R \cdot \frac{\delta\sigma}{E_s}(1 - \nu) = \frac{R^2}{2dE} \cdot (1 - \nu)\delta p \quad , \tag{35}$$

where E_s is the Young's modulus of the crust and ν the Poisson's ratio. If the debris bed is not in thermal balance, say, a fraction ξ of the decay heat in the molten interior goes to melting the crust, the mass of the crust that will be melted in time δt is

$$\frac{4\pi R^3}{3} \xi D \delta t \cdot \frac{1}{h_{s\ell}} \quad ,$$

where D is the power density and $h_{s\ell}$ the heat of fusion. The change in volume under constant pressure from solid to liquid is

$$\alpha \cdot \frac{4\pi R^3}{3} \cdot \xi D \cdot \frac{1}{\rho_s h_{s\ell}} \delta t \quad , \tag{36}$$

where $\alpha \simeq 0.15$, and ρ_s is the crust density. The change in volume inside the crust due to crust expansion is

$$4\pi R^2 \, \delta R = \frac{2\pi R^4}{dE_s}(1 - \nu)\, \delta p \quad , \tag{37}$$

so the volume of liquid inside the crust to be compressed is

$$\Delta V = \alpha \cdot \frac{4\pi R^3}{3} \cdot \xi D \cdot \frac{1}{\rho_s h_{s\ell}} \delta t - \frac{2\pi R^4}{dE_s} (1 - \upsilon) \delta p \quad . \tag{38}$$

Substituting Equation (38) and $V = (4\pi/3) R^3$ into Equation (34), we have

$$\delta p = \left[\frac{\alpha \xi D}{\rho_s h_{s\ell}} \delta t - \frac{3R}{2dE_s} (1 - \upsilon) \delta p \right] E_\ell \quad , \tag{39}$$

or

$$\frac{dp}{dt} = \frac{\alpha \xi D E_\ell}{\rho_s h_{s\ell}} \cdot \frac{1}{1 + 3RE_\ell (1 - \upsilon)/(2dE_s)} \quad . \tag{40}$$

At this point, we may want to recap the meanings of the symbols in Equation (40):

p	=	internal pressure of debris bed
α	=	fractional volume increase when solid debris melts at constant pressure (0.15)
D	=	power density of debris bed (1.5 MW/m^3)
ξ	=	fractional power of debris bed going into melting of the crust
E_ℓ	=	bulk modulus of molten debris
ρ_s	=	density of solid debris (9800 kg/m^3)
$h_{s\ell}$	=	heat of fusion of debris (2.7×10^5 J/kg)
R	=	radius of molten sphere

υ = Poisson's ratio of solid debris (0.32)

d = crust thickness

E_s = Young's modulus of solid debris (1.6×10^5 MPa).

The bulk modulus of liquid UO_2 is unknown. To estimate the pressure rise rate, we take (1) $E_\ell \simeq E_s/10$, and (2) $E_\ell >> E_s$. In the first case, we have

$$\frac{dp}{dt} \simeq \frac{\alpha \xi D E_s}{10\ \rho_s\ h_{s\ell}} \simeq 1.4\ \xi\ (\text{MPa/s}) \quad ; \tag{41}$$

and in the second case,

$$\frac{dp}{dt} \simeq \frac{2\alpha \xi D d E_s}{3\ \rho_s\ h_{s\ell}\ R(1 - \upsilon)} \simeq 13.3\ \xi\ \frac{d}{R}\ (\text{MPa/s}) \quad . \tag{42}$$

If the heat imbalance in the debris bed is about 10% of the decay heat ($\xi \simeq 0.1$), the pressure rise in both cases is about 0.1 MPa/s, and the increase rate of tangential stress on the crust is on the order of 1 MPa/s. With such a rapid increase in stress, the crust will have to crack almost constantly to relieve the internal pressure until a thermal steady-state is reached in the debris bed.

Instead of melting the crust, the molten interior could be solidifying onto the crust if net cooling of the debris bed was achieved by emergency core cooling water. The above formulas are still applicable in this case, but the sign of ξ is now negative.

Because the crust of the TMI-2 consolidated debris bed is believed to have failed after emergency cooling water was introduced into the core, leading to a reduction in pressure interior to the crust due to solidification, and also after a pressure reduction in the primary cooling system, leading to a reduction in pressure exterior to the crust, a

transient thermal calculation is needed to confirm if the internal pressure was indeed higher than the external pressure at the time of failure. Such a calculation requires the detailed knowledge of the configuration of the debris bed and the coolant conditions, both of which are quite uncertain. However, the thermal diffusion time, τ, across the crust is given by

$$\tau = \frac{\rho_s C_p d^2}{4k} , \tag{43}$$

where C_p is the specific heat, and k the thermal conductivity. Substituting the values

$$\rho_s = 9800 \text{ kg/m}^3$$

$$C_p = 500 \text{ J/kg-K}$$

$$k = 2.5 \text{ W/m-K},$$

we have

$$\tau \simeq 50 \, d^2 \text{ (s)} , \tag{44}$$

where d is measured in centimeters. If d was a few centimeters, the effect of cooling water would not have propagated to the molten pool at the time of crust failure some 20 min later. Therefore, solidification would not have occurred and the internal pressure would have remained high.

3.2.4 Collapse of the Upper Crust

With the relocation of molten material, the upper crust of the consolidated debris bed was no longer supported from below except along its periphery. The mass of rubble on top of the consolidated debris bed is estimated to be about 35,000 kg from post-accident examinations. The maximum stress, σ_m, on the crust due to the weight of the rubble is given by

$$\sigma_m = 0.75 \cdot \frac{mg}{\pi d^2} \quad , \text{(Reference 20)} \tag{45}$$

where m is the mass of the rubble, g the gravity, and d the thickness of the upper crust. It has been assumed that the load was distributed uniformly over the crust, which was in the form of a circular plate fixed at its edge. Numerically, σ_m is given by

$$\sigma_m = \frac{820}{d^2} \text{ (MPa)} \quad , \tag{46}$$

where d is to be expressed in centimeters.

If the upper crust was composed of homogeneous material solidified from a molten pool, its failure strength would be about 130 MPa. According to Equation (46), the crust would collapse if its thickness was less than about 2.5 cm. If the failure stress was reduced to 20 MPa due to the presence of cracks, the crust would collapse under the weight of the rubble if its thickness was less than about 6.4 cm. From the topography of the upper crust, which shows a concave surface at places (viewed from above), the crust indeed could have collapsed.

4. THERMAL INTERACTION BETWEEN MOLTEN CORE MATERIAL AND LOWER CORE SUPPORT STRUCTURES

As the molten core material flowed toward the lower plenum, it must have first vaporized the surrounding water and then itself might have broken up into droplets and solidified into granules. The voluminous production of steam, however, could have blanketed the molten core material that flowed down later. In this case, the molten material would have flowed down as a cohesive mass along the surfaces of the lower core support structures. If the contact time between the molten core material and the stainless steel structures in the lower plenum was short, thermal interactions between the materials were limited to a thin layer near the interface, and both materials could be considered infinite in extent in the thermal calculations. We shall first assume that the molten core material was at its melting point, so there was no heat transfer from the molten material to the surface where core material solidification took place. In this case, only heat conduction need be considered. If the molten material was heated above its melting point, convective heat transfer from the molten material to the solidifying surface also has to be considered. In the latter case, we shall estimate the conditions under which convective heat transfer may become important compared to heat conduction.

4.1 Contact Between Molten Core Material at its Melting Point and Stainless Steel

The heat conduction equation to be solved is

$$\frac{\partial T}{\partial t} = \alpha \frac{\partial^2 T}{\partial x^2} , \tag{47}$$

where T is the temperature, α the thermal diffusivity, t the time variable, and x the spatial variable. The geometry of the problem is shown in Figure 14. The steel is assumed to be at T_0 before contact, and the temperature at the contact surface, T_1, is assumed to be below the melting point of steel. (The latter assumption will be justified by the results of

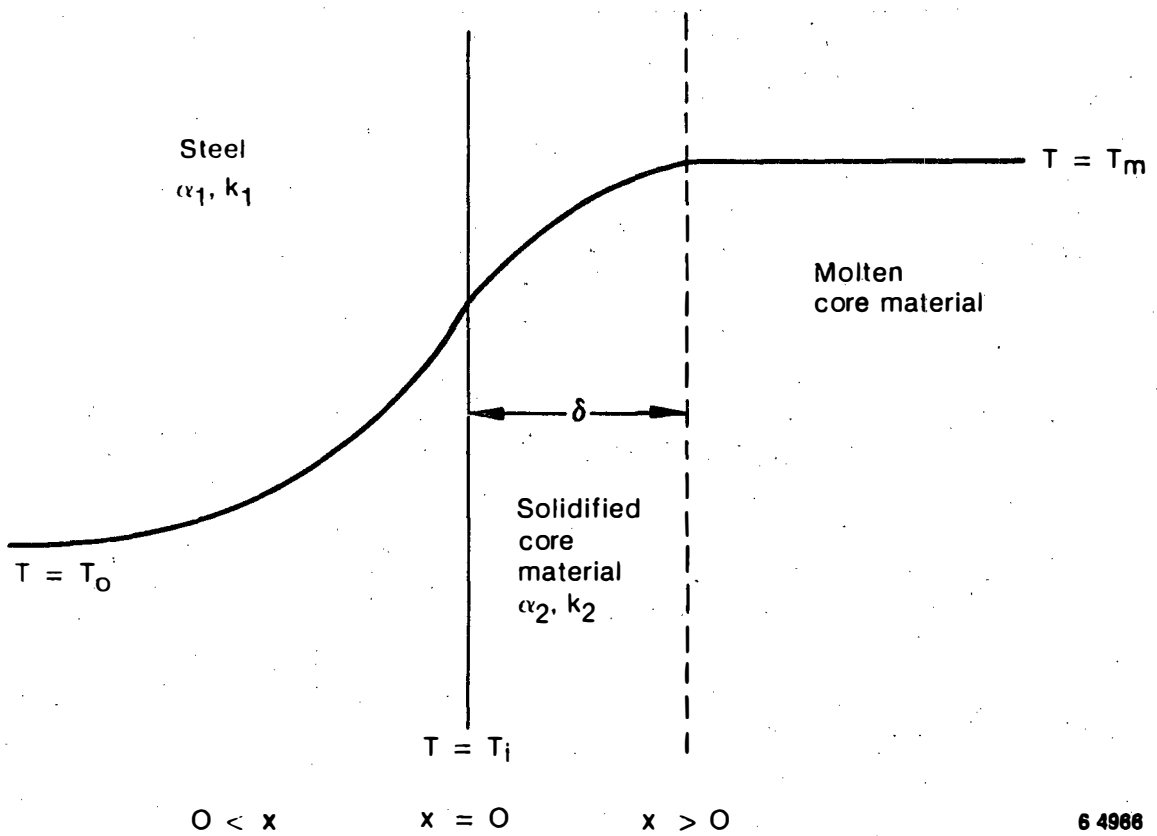

Figure 14. Thermal behavior of molten core material at its melting point in contact with steel below its melting point.

the calculation.) The molten core material is assumed to be at its melting point. We shall denote the thickness of the solidified layer by δ, which is to be determined from the solution.

The solution of Equation (47), satisfying the boundary conditions:

$$T(-\infty) = T_o, \text{ and } T(\delta) = T_m \quad , \tag{48}$$

is

$$T(x \leq o) = T_1 - (T_1 - T_o) \operatorname{erf}\left(-\frac{x}{2\sqrt{\alpha_1 t}}\right) ,$$

$$T(o \leq x \leq \delta) = T_1 + \frac{T_m - T_1}{\operatorname{erf}\left(\frac{\delta}{2\sqrt{\alpha_2 t}}\right)} \operatorname{erf}\left(\frac{x}{2\sqrt{\alpha_2 t}}\right) , \tag{49}$$

where T_1, the interface temperature, and δ, the solidified layer thickness, are determined by the following conditions:

$$k_1 \left(\frac{\partial T}{\partial x}\right)_{o^-} = k_2 \left(\frac{\partial T}{\partial x}\right)_{o^+} \quad , \text{ and} \tag{50a}$$

$$k_2 \left(\frac{\partial T}{\partial x}\right)_{\delta^-} = \rho \Delta H \frac{d\delta}{dt} \quad , \tag{50b}$$

where

k_1 = thermal conductivity of stainless steel

k_2 = thermal conductivity of solid core material

ρ = density of core material

ΔH = heat of fusion of core material.

The first condition gives heat flux continuity at the steel-core material interface, and the second condition balances the release of the heat of fusion to the heat conducted away from the interface of the solidified and molten core material.

If we make the substitution

$$\delta = 2\lambda \sqrt{\alpha_2 t} \quad , \tag{51}$$

where λ is a constant, Equations (50a) and (50b) yield the following equations for T_1 and λ:

$$T_1 = \frac{\dfrac{k_1}{\sqrt{\alpha_1}} T_o + \dfrac{k_2}{\sqrt{\alpha_2}\ \mathrm{erf}\ (\lambda)} T_m}{\dfrac{k_1}{\sqrt{\alpha_1}} + \dfrac{k_2}{\sqrt{\alpha_2}\ \mathrm{erf}\ (\lambda)}} \quad , \text{ and} \tag{52}$$

$$\lambda e^{\lambda^2} \left(\mathrm{erf}\ (\lambda) + \frac{k_2}{k_1} \sqrt{\frac{\alpha_1}{\alpha_2}} \right) = \frac{C_p\ (T_m - T_o)}{\sqrt{\pi}\ \Delta H} \quad , \tag{53}$$

where we have substituted the specific heat of the core material, C_p, from the relation

$$C_p = \frac{k_2}{\rho \alpha_2} \quad . \tag{54}$$

(We have neglected the density difference between the solid and molten core material.)

Equation (53) can be solved for λ using Newton's method which, when substituted into Equation (52), gives the interface temperature, T_1. The following numerical values are used in the solution:

k_1 = 25 W/m-K

$\alpha_1 = 6 \times 10^{-6}\ m^2/s$

$k_2 = 2.5$ W/m-K

$\alpha_2 = 5 \times 10^{-7}\ m^2/s$

$C_p = 500$ J/kg-K

$\Delta H = 2.7 \times 10^5$ J/kg

$T_m = 2800$ K

$T_o = 600$ K.

The solutions are

$\lambda = 0.898$, $\mathrm{erf}(\lambda) = 0.796$

$\delta = 1.27\sqrt{t}$ (mm), t in s

$T_1 = 1270$ K . (55)

The above solution shows that the interface temperature is indeed below the melting point of stainless steel. For an interface temperature above 1650 K (melting point of steel), parametric studies show that the initial temperature of the steel has to be above 1000 K, even if the melting point of the molten core material is raised to 3100 K.

4.2 The Effect of Convection in the Molten Core Material

If the molten core material was heated above its melting point, the convective heat flux from the main stream of the flow to the solidified layer generally cannot be neglected. If this convective heat flux is large, the solidification would slow down and eventually cease, limiting the extent of the solidified layer. Consequently, the steel-core material interface

temperature may increase beyond the melting point of steel. This section derives a lower limit on the time of contact that is required such that convective heat transfer becomes important.

From the last section, the heat flux going into the solidified layer is given by

$$\rho \Delta H \frac{d\delta}{dt} = \frac{\rho \Delta H \lambda \sqrt{\alpha_2}}{\sqrt{t}} = q_1'' \quad . \tag{56}$$

Let us assume that the molten core material was heated ΔT above its melting point. For Reynolds number on the order of a few hundred thousand and Prandtl number near 1, the average heat flux over a plate of length, L, in the direction of flow is given by

$$0.664 \frac{k_2}{L} \cdot \Delta T \cdot Pr^{\frac{1}{3}} Re^{\frac{1}{2}} = 0.664 \cdot \frac{\rho \alpha_2 C_p}{L} \cdot \Delta T \cdot Pr^{\frac{1}{3}} Re^{\frac{1}{2}} = q_2'' \quad , \tag{57}$$

where

$Pr = \frac{\nu_2}{\alpha_2}$ (Prandtl number)

$Re = \frac{uL}{\nu_2}$ (Reynolds number)

u = flow velocity

ν_2 = molten core material viscosity.

(We have neglected the difference in material properties between solid and molten core material.)

Convective heat transfer becomes important when

$$q_2'' > q_1'' \quad , \tag{58}$$

or

$$\sqrt{t} > \frac{L\rho\ \Delta H\ \lambda\ \sqrt{\alpha_2}}{0.664\ \rho\alpha_2\ C_p\ \Delta T\ Pr^{1/3}\ Re^{1/2}} = \frac{\lambda\ \Delta H}{0.664\ C_p\ \Delta T} \cdot Pr^{1/6} \cdot \left(\frac{L}{u}\right)^{1/2} \quad . \tag{59}$$

Substituting the following numerical values in Equation (59),

λ = 0.898

ΔH = 2.7×10^5 J/kg

C_p = 500 J/kg-K

Pr = 0.7,

we have the condition on the time of contact that convective heat transfer becomes important:

$$t > \frac{4.74 \times 10^5}{(\Delta T)^2} \cdot \frac{L}{u} \quad , \tag{60}$$

where ΔT is in K. We write Inequality (60) in a slightly different form:

$$ut > \frac{4.74 \times 10^5}{(\Delta T)^2} L \quad . \tag{61}$$

The left-hand side of Equation (61) may be considered as the length of the molten core material flow train. If ΔT is on the order of 100 K, the flow train has to be about 50 times the thickness of the lower core support plates (2.5 to 36 cm) for convective heat transfer to be important. For short flow trains, the conduction solution given in Section 4.1 should be adequate.

5. IMPLICATIONS OF THE VARIOUS FAILURE MECHANISMS

This section summarizes the results of the previous sections and discusses the implications of the various core debris bed failure mechanisms on the characteristics of the debris bed. Some of the characteristics can be verified by examinations of the debris bed and the reactor vessel internals, while others can be better defined through extended analysis of the accident.

Section 3.1.1 shows that the melt-through of a ceramic crust was not possible. The assumptions behind this conclusion are that (a) the consolidated debris bed had the dimensions indicated by the core examinations (0.9 m high and 1.2 m in radius), and (b) heat loss through the surface was uniform and was by radiation to a cool surface, such as water at saturation. We know that the top surface of the consolidated debris was covered with a rubble bed of shattered fuel and oxidized cladding. If this heat generating rubble was not quenched before crust failure, it would have insulated the top surface from radiating directly to the water. Given enough time, the top surface would indeed be melted by decay heat generation in the consolidated debris bed. Another way the surface of the consolidated debris bed could have melted is through nonuniform heat transfer from its interior. If the molten interior attained temperatures well above its melting point, convection in the molten pool would become significant and most of the heat generated in the pool would be transported to the side and top surfaces of the debris bed. Because the vertical and lateral dimensions of the debris bed were comparable, heat transfer patterns are difficult to obtain. If the local surface heat flux at some point was enhanced by an order of magnitude over the average surface heat flux, melt-through at that point could be achieved even for ceramic materials.

Rapid oxidation of a crust made of zircaloy was shown to be stable in Section 3.1.2 if the crust was already covered with a layer of zirconium dioxide more than 67 μm thick at the time when the crust reached rapid oxidation temperatures (>1600 K). Even with rapid oxidation, radiation loss from the surface to water would preclude surface melting. The crust could crack from thermal and mechanical stresses, allowing some molten zircaloy to

appear on the surface. The temperature of the surface could escalate in this case from the energy released in the oxidation of the fresh zircaloy, but due to the rapid buildup of an oxide layer, the escalation would be limited to only a few seconds. Careful examination of the breakthrough location on the crust may reveal if the crust was melted through from the outside, though the movement of molten material through the hole may complicate the interpretation of the examination.

A more plausible mechanism of a melt-through of the crust was presented in Section 3.1.3 where the effect of surface indentations on cutting down the heat loss was investigated. The presence of a relatively shallow cavity (twice as deep as wide) could lead to an equilibrium surface temperature at the melting point of UO_2. The initial melt-through of the crust, however, would be fairly localized, because the cavity is expected to be quite small, on the order of the diameter of a fuel or control rod. Relocation of more than ten metric tons of molten core material through the hole may take several tens of seconds, after allowing for enlargement of the hole from thermal ablation by the molten material at a temperature hundreds of K above its melting point.[21] The duration of the relocation of molten material to the lower plenum at 225 min was less than a minute, as indicated by the source-range monitor response (Figure 4). If the melt-through was due to this mechanism, the core material was either heated to a temperature many K above its melting point so rapid ablation and enlargement of a hole could take place, or there was simultaneous melt-through at several cavities.

A crust formed from the relocation of liquefied material, which solidified between fuel rods, could be relatively weak compared to a more uniform crust formed from the solidification from a molten pool. Section 3.2 showed that the expansion associated with melting of the crust from the interior before reaching thermal equilibrium would cause the crust to crack. The cracks would develop where the crust was weakest, possibly places where the crust was relatively thick but composed of inhomogeneous material (such as relocated UO_2 between fuel rods) or where the crust was relatively thin but formed from the solidification of a molten pool of UO_2 (such as at the upper surface of the consolidated debris bed). Thermal stress on the crust was also likely to crack its outer surface if it was

more than about 3 cm thick, though a complete crack across the crust was unlikely from thermal stresses alone. A positive pressure differential across the crust created by dropping the exterior system pressure, such as the one just before the hypothesized relocation at 225 min, may also lead to crust failure. Because there was essentially one such system pressure reduction after core damage, but before the relocation to the lower plenum at about 225 min, crust failure caused by such a pressure differential would have been a one-time event. On the other hand, cracking of the crust by thermal stress or by expansion of the interior through melting, could have occurred many times before relocation. In this case a question would arise as to why the cracks had been sealed before the 225-min event, but not at 225 min. Careful examination of the crust in terms of composition (metallic vs. ceramic), structure (homogeneity vs. heterogeneity), and geometry (thickness) may give indications of structural failure due to excessive stress. But the exact origin of the stress can only be found through detailed analysis of the thermal and mechanical behavior of the actual TMI-2 debris bed during the accident.

Section 4 presented a conduction solution of the thermal interaction of the molten core debris as it came in contact with the lower core support structures assuming that convective heat transfer in the molten material was negligible. For short durations of contact, on a time scale short compared to the thermal diffusion time in the stainless steel plates in the lower plenum (the conduction solution assumed infinite plates), the plates would be heated at their surface to about 1000 K. Some mechanical deformation at such a temperature is likely, but the mechanical loading on the plates has not been analyzed. Section 4 also derived a condition on the length of the flow train of the molten core material flowing past the steel plates such that convective heat transfer became important. For superheat of about 100 K above its melting point, the flow train had to be about 50 times the thickness of the plates before convective heat transfer could become significant. For shorter flow trains, the conduction solution stands, so there would not have been thermal damage to the structures. Examinations of the lower core support structures so far show that the damage was absent or minimal, so the flow train could have been relatively short.

In this report, we have examined some of the thermal and mechanical conditions under which the crust of a non-coolable mass formed in the reactor core could fail to allow its molten interior to flow to the lower part of the reactor vessel. The failure mechanism of the TMI-2 non-coolable mass in the core, however, cannot be determined precisely without a detailed transient thermal and mechanical analysis of the damaged core. Such an analysis requires the knowledge of the hydraulic conditions in the core and the material properties at high temperatures, both of which can at best be estimated only, so the results of the analysis may not be unambiguous. A more fruitful way to determine the failure mechanism is through careful examination of the geometry of the debris and testing the remnants of the crust for their thermal and mechanical properties, preferably at high temperatures. These efforts may ultimately help define the precise failure mechanisms.

Regardless of the initial failure mechanism of the crust, analysis and examination of the reactor core and vessel internals thus far indicate that molten core material broke out of the crust and relocated to the lower plenum, leading to a collapse of a crust holding the loose rubble in the upper part of the core. During its flow to the lower plenum, the molten core material caused little, if any, damage to the lower core support structures.

6. REFERENCES

1. C. M. Allison, S. T. Polkinghorne, and M. S. Sohal, SCDAP/MOD1 Analysis of the Progression of Core Damage During the TMI-2 Accident, EGG-SAR-7104, November 1985.

2. R. K. McCardell et al., Severe Fuel Damage Test Series, Severe Fuel Damage Scoping Test Quick Look Report, EG&G Idaho, Inc., December 1982.

3. R. K. McCardell et al., Severe Fuel Damage Test 1-1 Quick Look Report, EG&G Idaho, Inc., October 1983.

4. R. W. Miller et al., Severe Fuel Damage Test 1-3 Quick Look Report, EG&G Idaho, Inc., October 1984.

5. R. W. Miller et al., Severe Fuel Damage Test 1-4 Quick Look Report, EG&G Idaho, Inc., July 1985.

6. P. Kuan, TMI-2 Core Debris Bed Coolability, EGG-TMI-7150, March 1986.

7. R. Gold et al., Solid-State Recorder Neutron Dosimetry in the Three Mile Island Unit-2 Reactor Cavity, GEND-INF-059, May 1985.

8. A. J. Baratta, B. R. Bandini, and M. L. Gundy, "Estimation of Fuel Distribution in TMI-2 Reactor Vessel," in TAGG (TMI-2 Technical and Advisory Group) Planning Study, Fuel Conditions and Locations, TPO/TMI-166, Rev. 0, April 1985.

9. D. J. N. Taylor, TMI-2 Self-Powered Neutron Detector Data Interpretation, EG&G Idaho draft report, February 1986.

10. M. E. Yancey et al., TMI-2 In-Core Instrument Damage--An Update, GEND-INF-031, Volume II, April 1984.

11. R. E. Pawel, J. V. Cathcart, and R. A. McKee, "The Kinetics of Oxidation of Zircaloy-4 in Steam at High Temperatures," Electrochemical Science and Technology, Vol. 126, No. 7, July 1979.

12. V. F. Urbanic and T. R. Heidrick, "High-Temperature Oxidation of Zircaloy-2 and Zircaloy-4 in Steam," Journal of Nuclear Materials, 75(1978), pp. 251-261.

13. M. Perlmutter and R. Siegel, "Effect of Specularly Reflecting Gray Surface on Thermal Radiation Through a Tube and from its Heated Wall," J. Heat Transfer, Trans. ASME, Series C, Vol. 85, pp. 55-62, 1963.

14. A. A. Griffith, Phil. Trans Roy. Soc., A221, pp. 163-198, 1921.

15. H. M. Westergaard, J. Applied Mechanics, A, 49, June 1939.

16. J. F. Knott, Fundamentals of Fracture Mechanics, Chapters 3 and 4, John Wiley and Sons, New York, 1979.

17. D. L. Hagrman, G. A. Reymann, and R. E. Mason, MATPRO-Version 11 (Rev. 2), A Handbook of Materials Properties for Use in the Analysis of Light Water Reactor Fuel Rod Behavior, NUREG/CR-0479, August 1981.

18. D. P. H. Hasselman, "Analysis of the Strain at Fracture of Brittle Solids with High Densities of Microcracks," J. American Ceramic Society, Vol. 52, No. 8, p. 458, August 1969.

19. S. P. Timoshenko and J. N. Goodier, Theory of Elasticity, Third Edition, p. 436, McGraw-Hill Book Company, 1970.

20. T. Baumeister and L. S. Marks, Standard Handbook for Mechanical Engineers, pp. 5-68, 5-69, Seventh Edition, McGraw-Hill Book Company, 1967.

21. TMI-2 Core Material Motion--Development of the Cavity Model, Fauske and Associates, Inc, Report submitted to EG&G Idaho, Inc., FAI/86-12, April 1986.

APPENDIX A

POWER DENSITY IN THE CONSOLIDATED DEBRIS BED

APPENDIX A

POWER DENSITY IN THE CONSOLIDATED DEBRIS BED

Below 2700 K, based on the U-Zr-O equilibrium phase diagram, the molar ratio of Zr to UO_2 is 4:1, and the mass ratio is 0.57:0.43. In a fuel rod, the mass fraction of fuel is 0.80. Since the fuel rods occupy a fraction of 0.45 of the core volume, the liquefied core material will occupy 0.55 of the volume of a consolidated debris bed formed from its solidification between fuel rods. The mass fraction of UO_2 in the consolidated debris bed is therefore (0.80 x 0.45 + 0.43 x 0.55), or 0.60. Assuming a UO_2 density of 10,000 kg/m^3, and a zircaloy density of 6500 kg/m^3, the average density of the consolidated debris bed is 8230 kg/m^3. The mass of UO_2 per unit volume of the consolidated debris bed is 4940 kg/m^3.

Two hundred (200) min after reactor shutdown the decay power of the TMI-2 core was about 23 MW, and the average decay power per unit mass of UO_2 was 0.25 kW/kg. If 50% of the volatile fission products was released from the fuel in the consolidated debris bed, the decay power would be reduced by 12%. Assuming a power peaking factor of 1.35 in the central part of the core where the consolidated debris bed was formed, the power density in the debris bed was (0.88 x 1.35 x 0.25 x 4940) kW/m^3, or 1.47 MW/m^3.